Insight into ultrasound-mediated reactive oxygen species generation by various metal-porphyrin complexes

Francesca Giuntini[a], Federica Foglietta[b], Arianna M. Marucco[c], Adriano Troia[d], Nikolai V. Dezhkunov[e], Alessandro Pozzoli[a], Gianni Durando[d], Ivana Fenoglio[c], Loredana Serpe[b]*, Roberto Canaparo[b]

[a]School of Pharmacy and Biomolecular Sciences, Liverpool John Moores University, Liverpool L3 2AJ, UK

[b]Department of Drug Science and Technology, University of Torino, Via Pietro Giuria 13, 10125 Torino, Italy

[c]Department of Chemistry, University of Torino, Via Pietro Giuria 7, 10125 Torino, Italy

[d]National Institute of Metrological Research (INRIM), Strada delle Cacce 91, 10135 Torino, Italy

[e]Belarusian State University of Informatics and Radioelectronics (BSUIR), P. Brovka St.6, 220013, Minsk, Belarus

***Corresponding author**:

Loredana Serpe, MD PhD

Department of Drug Science and Technology, University of Torino

Via Pietro Giuria 13, 10125 Torino, Italy,

Phone: +39 011 6706235 Fax: +39 011 6706230 e-mail: loredana.serpe@unito.it

Abstract

Ultrasound is used to trigger the cytotoxicity of chemical compounds, known as sonosensitisers, in an approach called sonodynamic therapy (SDT), which is under investigation herein. The generation of reactive oxygen species (ROS) has been proposed as the main biological occurrence that leads to the cytotoxic effects, which are achieved via the synergistic action of two components: the energy-absorbing sonosensitiser and ultrasound (US), which are both harmless *per se*. Despite some promising results, a lack of investigation into the mechanisms behind US sonosensitiser-mediated ROS generation has prevented SDT from reaching its full potential.

The aim of this work is to investigate the US-responsiveness of a variety of metal-porphyrin complexes, free-base porphyrin and Fe(III), Zn(II) and Pd(II) porphyrin, by analyzing their ROS generation under US exposure and related bio-effects. All experiments were also carried out under light exposure and the results were used as references.

Our results show that porphyrin ultrasound-responsiveness depends on the metal ion present, with Zn(II) and Pd(II) porphyrin being the most efficient in generating singlet oxygen and hydroxyl radicals. ROS production efficiency is lower after ultrasound exposure than after light exposure, because of the various physico-chemical mechanisms involved in sensitiser activation. US and porphyrin-mediated ROS generation is oxygen-dependent and the activation of porphyrin by US appears to be more compatible with sonoluminescence-based photo-activation rather than a radical path process that occurs via the homolytic bond rupture of water. Notably, the cytotoxicity results reported herein, which are mirrored by *ex-cellulo* data, confirm that the type of ROS generation achieved by the US activation of intracellular porphyrins is pivotal to the effectiveness of cancer cell killing.

Keywords: Porphyrin; Ultrasound; Reactive oxygen species; Sonodynamic therapy; Cancer

INTRODUCTION

Sonodynamic therapy (SDT) is a proposed therapeutic approach based on the synergistic effect between a suitable chemical compound (sonosensitiser) and low intensity ultrasound (US), which is used to kill cancer and microbial cells [1, 2]. The effectiveness of SDT has been demonstrated in *in vitro* and *in vivo* animal models [3-10], although the underlying sonosensitization mechanism is still not fully understood.

It is widely accepted that the biological effects elicited by US (in pulsed or continuous mode) are predominantly due to one or a combination of the following factors: i) heat generation [11], ii) sonoporation [12], iii) cell membrane rupture [13], and iv) free radical generation [14]. The last of these is thought to play the predominant role in SDT [15]. It has been proposed that some US-mediated biological effects rely on the occurrence of acoustic cavitation [16]; a phenomenon that involves the nucleation and growth of gas-filled bubbles in a liquid milieu exposed to an appropriate US field. In this phenomenon, bubbles in a state of stable (non-inertial) cavitation oscillate, causing streaming and mixing in the surrounding liquid/medium, whereas gas bubbles in inertial cavitation grow to near resonance size and expand to a maximum before collapsing violently [17]. In this latter case, the energy released by bubble implosion, referred to as a "sonochemical reactor", generates flashes of light known as sonoluminescence (SL), whose UV/visible emission spectra have been found to indicate the presence of high local temperatures (from 5000 up to 15000 °K) and pressures associated with bubble collapse [15, 18-21].

Acoustic cavitation is a highly complex phenomenon that is not yet completely understood despite being well known in a variety of scientific fields, from physics to chemistry and medicine. For some researchers, acoustic cavitation is an extreme phenomenon that is responsible for generating excessive vibration, erosion, reduced hydraulic performance and structural damage [22], while, for others, it is seen as an enormous concentration of energy with a wide range of unexplored chemical and physical consequences [23, 24]. In particular, the emission of SL [25-27] has been proposed as

the pivotal trigger for the sonosensitiser-mediated generation of reactive oxygen species (ROS) in SDT [28, 29]. This hypothesis was formulated because most of the chemical compounds used in SDT are also photosensitisers [14]. It has therefore been suggested that the mechanism that underlies SDT is similar to the one behind photodynamic therapy (PDT) [30]. Moreover, this hypothesis is consistent with the idea that sonodynamic activity may predominantly take place inside cells and that singlet oxygen may play an important role in eliciting sonodynamic cytotoxicity. Even though this hypothesis has created some consensus, doubts have been expressed as to the occurrence of intracellular acoustic cavitation. Nevertheless, this idea has fostered some support thanks to indirect evidence, including reports of sonodynamic cancer cell death occuring in cancer cells exposed to aminolevulinic acid [31-33], a pro-drug capable of augmenting the intracellular pool of the sonosensitiser protoporphyrin IX, and the scavenger-mediated identification of singlet oxygen [29, 34]. Moreover, efficient cancer cell killing by SDT has been achieved using sensitisers of very diverse molecular structure, including porphyrins and tetrapyrroles, non-steroidal anti-inflammatory drugs, xanthenes and anticancer drugs [35, 36]. The chemical heterogeneity of the sonosensitizing species naturally leads to the assumption that sonosensitiser structure has no central role to play in STD and that they are simply a tools that can produce longer-lived free radicals and other highly reactive species under acoustic cavitation in order to kill cancer cells, predominantly by damaging the cell membrane. Therefore, although it is generally agreed that the generation of free radicals is the main cause of sonodynamic cancer cell killing, there is less consensus as to the underpinning mechanism behind reactive species generation (intracellular acoustic cavitation and/or sonoluminescence occurrence), the role of the sonosensitiser in ROS production, the kind of reactive species produced and where sonodynamic processes take place (inside or outside the cells).

With this in mind, we have undertaken this study with the aim of elucidating the influence that a series of water-soluble metalloporphyrins used under US and light exposure (for reference

purposes) have on ROS generation, in an attempt to identify the relationship between porphyrin-mediated ROS generation efficiency and sonodynamic activity. The investigation characterised the generation of ROS by the various metalloporphyrins under US and light exposure, monitored sonoluminescence occurrence and evaluated the anticancer activity of the metalloporphyrins on the colorectal cancer cell line, HT-29, under US and light exposure. Experiments were also carried out on the human dermal fibroblast cell line, HDF, in order to evaluate the effects that the treatment had on non-cancerous cells.

MATERIALS AND METHODS

Synthesis

Reagents were purchased from Sigma-Aldrich (UK), Fisher Scientific (UK) and Fluorochem (UK). Solvents were obtained from Fisher (UK). All reagents and solvents were used as supplied without further purification. Porphyrins **1**-**4** (Fig. 1) were synthesized according to methods previously reported in the literature, with some modifications [37]. NMR spectra were recorded using a Bruker Avance 300 spectrometer at 300.1 MHz (^{1}H NMR) and 75.5 MHz (^{13}C NMR) (see Supplementary Materials, Fig. S1). Spectra were recorded in d_6-DMSO (Fluorochem, UK) and chemical shifts were determined relative to the residual solvent peaks at δ = 2.51 (^{1}H NMR) and δ = 39.6 ppm (^{13}C NMR). Q-TOF-MS data were acquired in positive mode by scanning from 400 to 3000 *m/z* without auto MS/MS fragmentation. Ionisation was achieved using an Agilent JetStream electrospray source and infused internal reference masses. Agilent 6540 Q-TOF-MS parameters were as follows: a gas temperature of 325 °C, a drying gas flow rate of 10 L/min and a sheath gas temperature of 400 °C were used. UV-visible spectra were recorded on a Varian Cary 50 UV/vis spectrophotometer (wavelength accuracy: ± 0.24 nm). Fluorescence spectra (uncorrected) were recorded on a Cary Eclipse Fluorimeter.

*5,10,15,20-tetrakis(N-methylpyridinium-4-yl)porphyrin tetrachloride (**1**)*. Methyl iodide (2 mL, 32.11 mmol) was added to a solution of 5,10,15,20-*tetrakis*-(4-pyridyl)porphyrin (500 mg, 0.80 mmol) in *N*-methylpyrrolidinone (100 mL). The resulting solution was stirred at 40 °C for 12 h. Reaction mixtures were then allowed to cool to room temperature and were treated with diethyl ether (300 mL). The supernatant was decanted and the precipitate was washed three more times with diethyl ether and the supernatant was decanted each time. The solid was dissolved in water and the resulting solution was treated with 10% aqueous NH_4PF_6 (5 mL). The solid was recovered by centrifugation, dissolved in acetone and treated with 10% tetrabutylammonium chloride in acetone

(2 mL). The precipitate was collected by centrifugation and crystallised from methanol and diethyl ether to yield the desired compound (855 mg, 82%). Spectroscopic data were in agreement with the data reported in the literature.

General procedure for metal insertion into compound 1

*5,10,15,20-tetrakis(N-methylpyridinium-4-yl)porphyrinato iron(III) pentachloride (**2**).* The compound was obtained via the procedure described above, with the only difference being that the reaction mixture was kept at 40 °C for 10 h. Compound **2** was obtained in 76% yield. Spectroscopic data were in agreement with data reported in the literature [37]. ESI-MS^+: $[M\text{-}4Cl]^{4+}/4$, 190.78

*5,10,15,20-tetrakis-(N-methylpyridinium-4-yl)porphyrinato zinc(II) tetrachloride (**3**).* A solution of **1** (208 mg, 0.25 mmol) in water (240 mL) was treated with $Zn(OAc)_2 \cdot 2H_2O$ (280 mg, 1.27 mmol) at room temperature. The mixture was stirred at room temperature until complete conversion was achieved (monitored by UV-visible spectroscopy and MS spectrometry). It was then diluted with water (80 mL) and treated with 10% aqueous NH_4PF_6 (2 mL). The solid was recovered by centrifugation, dissolved in acetone (30 mL) and treated with 10% tetrabutylammonium chloride in acetone (2 mL). The precipitate was collected by centrifugation and crystallised from methanol and diethyl ether to yield the desired compound (188 mg, 84%). Spectroscopic data were in agreement with data reported in the literature [37]. ESI-MS^+: $[M\text{-}4Cl]^{4+}/4$, 185.03

*5,10,15,20-tetrakis(N-methylpyridinium-4-yl)porphyrinato palladium(II) tetrachloride (**4**).* The compound was obtained via the procedure described above, with the only difference being that the reaction mixture was kept at 40 °C for 10 h. Compound **4** was obtained in 78% yield. Spectroscopic data were in agreement with data reported in the literature [38]. ESI-MS^+: $[M\text{-}4Cl]^{4+}/4$, 195.02

Electron spin resonance spectroscopy

ROS generation was monitored using electron spin resonance (EPR) spectroscopy (Miniscope 100 EPR spectrometer, Magnettech, Germany) and the spin trapping technique, which used DMPO (5,5-dimethyl-1-pyrroline-N-oxide, Alexis Biochemicals, USA) and 4-oxo-TMP (2,2,6,6-tetramethyl-4-piperidone, Sigma-Aldrich) as the spin-probing agents for oxygen radicals and singlet oxygen, respectively. All the other reagents were obtained from Sigma-Aldrich. Ultrapure Milli-Q water (Millipore, Billerica, USA) was used.

Sample preparation. 600 μL of a 0.4 mM aqueous porphyrin solution were diluted in 1.9 mL of a phosphate buffered saline solution (PBS) containing either DMPO (50 mM), for the hydroxyl/superoxide radical, or 4-oxo-TMP (50 mM) for singlet oxygen. The solution was either irradiated using a HgXe lamp in quartz vials for 5 min or exposed to US in a polystyrene tube for 5 min. EPR spectra were recorded, using 50 μL of the solution, immediately after treatment. In one case, the experiment was also repeated after by bubbling the solution with Ar in a controlled atmosphere to remove dissolved oxygen for the duration of US exposure. Simulations of EPR experimental signals were performed using Winsim 2002 software (National Institute of Environmental Health Science, National Institutes of Health, USA). Hyperfine splitting constants, obtained from an optimization of the simulation, were compared with those reported in the literature (NIESH STBD database).

Ultrasound exposure. The US field was generated using a plane wave transducer (2.54 cm diameter), operating in continuous wave mode at f = 1.866 MHz, that was connected to a power amplifier (Type AR 100A250A; Amplifier Research, Souderton, USA) and a function generator (Type 33250; Agilent, USA). A custom-built mechanical adaptor was connected to the 1 cm diameter polystyrene tube containing the solution. When filled with ultrapure water, the adaptor guarantees the high reproducibility of measurement conditions [39]. The distance from the transducer to the cell tube was set at 17 mm. US exposure was performed for 5 min under subdued

light at a US power of 1.5 W/cm^2. The maximum temperature recorded in the US exposed sample was 33 °C.

Light exposure. A 500 W Hg/Xe lamp (Oriel Instruments, USA), was used with a 400 nm cut-off filter and an IR water filter to avoid suspension overheating. Light irradiance in the visible region was measured using a Deltahom instrument (Italy) equipped with a detector operating in the UVA and visible/NIR ranges (400-1050 nm). An irradiance of 51.8 mW/cm^2 was measured in all experiments. Irradiation was carried out for 5 min.

Sonoluminescence measurements

In order to collect the light emitted from the bubble cloud that was generated by the ultrasonic transducer, the transducer itself inserted into the bottom of a Plexiglas tube (diameter: internal 30 mm, external 40 mm; Techno Plastic Products, Switzerland) filled with either 30 mL of 2 μM porphyrin in aqueous solution or with aqueous solution alone (control). The tube was inserted into a dark chamber at a constant temperature of 10°C (± 1°C). The emitted light was acquired by two quartz lenses, positioned at the top of the Plexiglas tube, that were coupled to a multicore UV-visible optical fibre connected to a monochromator (Acton SP 300i, Princeton Instruments, USA). Spectra (200-700 nm) were recorded using an LN cooled CCD (XDX mode l, Princeton Instruments) and were acquired over 3 min at a resolution of 1 nm [40]. Since SL emission decreases as the temperature of the liquid rises (a frequently observed phenomenon in liquids exposed to high-frequency US), we measured the temperature of the solution after each SL acquisition. The maximum temperature measured, using a needle thermocouple, was 35 °C, which is consistent with the experimental conditions for cell treatment. To improve the signal to noise ratio (S/N) of SL, experiments were also carried out while bubbling Ar in air-equilibrated solution for the duration of US exposure [41].

Cell proliferation assay

The human colorectal cancer cell line, HT-29 (Interlab Cell Line Collection, Italy), was cultured in McCoy's 5A medium (Sigma-Aldrich) and the human dermal fibroblast cell line, HDF (ECACC, Salisbury, UK), was cultured in DMEM (Sigma Aldrich). All media were supplemented with 10% FBS (Lonza, Belgium), 2 mM L-glutamine, 100 UI/mL penicillin and 100 µg/mL streptomycin (Sigma-Aldrich) and maintained in a dark incubator (Thermo Fisher Scientific, USA) in a humidified atmosphere of 5% CO_2 air at 37 °C. At 85% confluence, cells were harvested with 0.05% trypsin-0.02% EDTA solution (Sigma-Aldrich), suspended once again in culture medium and seeded at the appropriate cell concentration for the experiment.

In the exponential growth phase, cells were pre-incubated in the dark for 24 h with porphyrins. The cells were then normalized to 5×10^5 cells in a polystyrene tube filled with phosphate buffered saline (PBS), at pH 7.4, for sonodynamic and photodynamic treatment.

The *in vitro* sonodynamic experiments were performed under subdued light and the temperature of the medium was controlled to avoid hyperthermia during the experiment.

After treatment, 2.5 x 10^3 cells were seeded in 100 µL of culture medium in replicates (n=8) in 96-well culture plates. 10 µL of WST-1 solution (Roche Applied Science, Germany) was added at 24, 48, and 72 h and the plates were incubated at 37°C in 5% CO_2 for 1.5 h for HT-29 cells and for 2 h for HDF cells. Well absorbance was evaluated at 450 and 620 nm using a microplate reader (Asys UV340; Biochrom, UK). Cell proliferation data were expressed as a percentage of untreated cells.

Confocal microscopy

The uptake of porphyrins **1-4** by HT-29 cells was investigated using confocal microscopy to provide qualitative evidence for their intracellular localization. 2 x 10^5 HT-29 cells were left to attach for 24 h on glass coverslips in 24-well plates and were then incubated for 24 h with porphyrins **1**, **2** and **4** and with porphyrin **3** at 500 and 250 µM, respectively. At the end of the

incubation time, slides were fixed with 4% paraformaldehyde (Sigma-Aldrich) for 15 min and cell nuclei were then stained with TO-PRO®-3 (Thermo Fisher Scientific) for 15 min. Images were acquired using a Leica TCS SP5 AOBS confocal system (Leica Microsystems, Italy) equipped with a 405 nm diode, an Ar ion and a 633-nm HeNe laser. Fixed cells were imaged using a HCX PL APO 40x 1.25 NA oil immersion objective at a pixel resolution of 0.094 × 0.094 μm.

***In vitro* sonodynamic and photodynamic treatments**

HT-29 cells in the exponential growth phase were incubated for 24 h with culture medium containing porphyrins (**1**, **2** and **4** at 500 μM; **3** at 250 μM) in a dark incubator. The porphyrin concentrations for the SDT and PDT treatments were set at the highest non-cytotoxic concentration obtained from the cell proliferation curves, which were carried out 24 h after incubation with various porphyrin concentrations (125, 250, 500 and 1000 μM). Moreover, in order to investigate the dependency that the sonodynamic cytotoxicity has on porphyrin dose, treatments were also carried out over increasing porphyrin concentrations. After the sonodynamic and photodynamic treatments, 2.5 x 10^3 cells were plated in a 96-well culture plates and cell proliferation was evaluated using the WST-1 assay 24, 48 and 72 h after treatment, as previously described.

Sonodynamic treatment. After incubation, cells were washed with PBS, trypsinized and normalized to 5.0 x 10^5 cells in 2.5 mL PBS in polystyrene tubes for US exposure. Cells were exposed to US using the settings described above.

Photodynamic treatment. After incubation, cells were washed with PBS, trypsinized and normalized to 5.0 x 10^5 cells in 2.5 mL of PBS in polystyrene tubes (Techno Plastic Products) to ensure light exposure. Each cell tube was then irradiated in a dark box using the settings described above.

ROS scavenging assay. HT-29 cells were incubated with the ROS scavenger N-acetyl-cysteine (NAC; Sigma) in order to evaluate the role that ROS play in the cytotoxicity induced by the

exposure of porphyrin-incubated cells to US. Briefly, cells were incubated with porphyrins (either **3** at 250 μM or **4** at 500 μM) for 24 h and 5.0 mM NAC was added for the last 3 h of porphyrin incubation. Cells were then trypsinized, washed with PBS and exposed to US, using the settings described above. Cell growth was assessed using a WST-1 assay after 24, 48 and 72 h.

Treatment of non-cancerous cells. HDF cells were incubated with the porphyrins and exposed to either US or light to evaluate the effects of the treatments on cell growth. Briefly, cells were incubated with porphyrins (either **3** at 250 μM or **4** at 500 μM) for 24 h, washed with PBS, trypsinized, normalized to 1.0 x 10^5 cells in 2.5 mL PBS in polystyrene tubes and exposed to either US or light, using the settings described above. Cell growth was assessed using a WST-1 assay after 24, 48 and 72 h.

Flow cytometry

ROS generation and cell death were assessed using flow cytometric assays on a C6 flow cytometer (Accuri Cytometers, USA). Sonodynamic and photodynamic ROS production was measured using 2,7-dichlorofluorescein diacetate (DCF-DA, Molecular Probes, USA) as the intracellular probe for oxidative stress. DCFH-DA is a stable, non-fluorescent molecule that readily crosses the cell membrane and is hydrolysed by intracellular esterases to form the non-fluorescent DCFH, which is itself oxidized in the presence of peroxides to form the highly fluorescent 2,7-dichlorofluorescein (DCF) upon oxidation by ROS. Incubation with porphyrins was carried out as described above. Cells were then incubated with 10 μM DCFH-DA for 30 min. Following DCFH-DA incubation, cells were washed with PBS, trypsinized, normalized to 5 x 10^5 cells, collected in 2.5 mL of PBS and subjected to either sonodynamic or photodynamic treatment. ROS production was assessed 1, 5, 15, 30 and 60 min after treatment. 10,000 events were considered in the analysis. ROS production is expressed as the integrated median fluorescence intensity (iMFI), which was calculated as the product of the frequency of ROS-producing cells and the median fluorescence

intensity of the cells. The iMFI ratio was calculated in order to provide information on the ratiometric variation in fluorescence per time point with respect to control cells (untreated cells). ROS detection was stopped when the iMFI ratio started to decrease, because of the significant increase in DCF fluorescence in control cells [42], in order to limit any assay artifacts that may influence evaluations of the real intracellular ROS content, as induced by the investigated treatments.

Cell death was evaluated using the Dead Cell Apoptosis Kit, with Annexin V-Alexa Fluor® and propidium iodide (PI, Life Technologies, Italy) 24 h after treatment. Cells were detached with trypsin, washed with PBS at 1,500 rpm for 5 min and then re-suspended with 1x Annexin-binding buffer and stained with Annexin V-Alexa Fluor® and PI. Sample analyses were carried out at 488 nm excitation to measure Annexin V-Alexa Fluor® and at 530 nm to measure PI. 10,000 events were considered in the analyses and any cell debris that displayed low forward light scatter and side light scatter was excluded from the analyses. The two different staining types allowed us to identify the presence of apoptotic (Annexin V-Alexa Fluor® positive) and necrotic cells (Annexin V-Alexa Fluor® and PI positive) and tell them apart from viable cells (Annexin V-Alexa Fluor® and PI negative). All analyses were performed using FCS Express software version 4 (BD Bioscience, Italy).

Transmission electron microscopy

Samples for ultrastructural evaluation were fixed in 2.5% gluteraldehyde phosphate (pH 7.3) and stored at 4 °C for 24 h. After the post-fixation process (1% osmium for 2 h followed by a quick wash out in 30% acetone), the samples were dehydrated in acetone and embedded in Spurr resin. Thin sections (0.90 μm) were obtained from each sample using an ultramicrotome, they were then stained with toluidine blue and ultrathin sections (70 nm) were contrasted with uranyl acetate and lead citrate. The grids were evaluated using a Philips CM10 transmission electron microscope.

Statistical analysis

Data are shown as mean values ± standard deviation of three independent experiments. Statistical analyses were performed on Graph-Pad Prism 6.0 software (La Jolla, USA). Two-way analysis of variance and Bonferroni's test were used to calculate the threshold of significance. The statistical significance threshold was set at $p < 0.05$.

RESULTS

Identification of ROS produced by the sonodynamic or photodynamic activation of porphyrins

ROS generation can be monitored using a combination of electron paramagnetic resonance (EPR) spectroscopy and spin trapping; a powerful technique that is able to both identify and quantify the presence of paramagnetic species [43]. In fact, specific spin traps were used to monitor the generation of superoxide radicals ($O_2^{\bullet -}$), hydroxyl radicals ($HO^{\bullet}$) and singlet oxygen ($^1O_2$) in this work. The EPR signals obtained using the spin traps DMPO (panel A) and 4-oxo-TMP (panel B), after the exposure of aqueous solutions of porphyrins **1**-**4** to US, are shown in Fig. 2. Whereas no signals were observed in the absence of porphyrins and US exposure (see Supplementary Materials, Fig. S2), a four line signal ($a^N = a^H$ 14.4G), which corresponds to the paramagnetic adduct DMPO/$OH^{\bullet}$, was observed in the presence of all porphyrins. Porphyrin **3** gave the highest signal intensity, indicating that it has the highest hydroxyl radical generation efficiency (Fig. 2A). Moreover, in order to confirm that the OH originates from molecular oxygen, EPR analyses were carried out in an Ar-saturated solution and in a controlled atmosphere to remove dissolved oxygen for the duration of US exposure, and highlighted the absence of the OH (see Supplementary Materials, Fig. S3).

In the presence of the singlet oxygen trap, 4-oxo-TMPO, a clear three peak EPR signal (a^N 15.8 G) was observed in all samples following US exposure, while a marginally more intense signal was found in the porphyrin **4** sample (Fig. 2B). This signal indicates the presence of the radical TEMPONE that is formed via the reaction between singlet oxygen and the probe 4-oxo-TMP [44-46].

The same experiments were performed under light irradiation (Fig. 3) in order to verify whether the ROS obtained from US exposure are also generated by photodynamic processes, and it was found

that all porphyrins showed comparable singlet oxygen generation efficiency (Fig. 3B). However, a different, seven-line signal, which was particularly intense with porphyrin **2**, was observed when DMPO was used (Fig. 3A). A simulation of this signal (SI) revealed two splitting constants, one (3.9 G) involving two nuclei of nuclear spin 1/2 and the other (7.1 G) involving a nucleus of nuclear spin 1 (Fig. S4). This pattern corresponds to a previously identified DMPO decomposition product (DMPOX) [47].

Sonoluminescence occurrence during the sonodynamic activation of porphyrins

The EPR ROS identification results, drove us to investigate the occurrence of SL during the US exposure of porphyrins **3** and **4**, which showed the highest US-responsiveness (Fig. 2). Typical SL broad band emissions were observed in all the tested solutions (Fig. 4). The air-equilibrated solutions were flushed with Ar during US exposure to increase the SL S/N ratio (see Supplementary Materials, Fig. S5). Notably, an additional emission, which corresponds to $OH(A^2\Sigma^+ - X^2\ \Pi_{[1/2,3/2]})$ radical emission from vibrational bands [41], was observed around 310-340 nm in the porphyrin **3** solution.

Cytotoxicity induced by the sonodynamic and photodynamic activation of porphyrins

All porphyrins were taken up by HT-29 cells and principally showed cytoplasmic distribution after 24 h of incubation (Fig. 5).

The effects of sonodynamic and photodynamic treatment on HT-29 cell growth, at the highest non-cytotoxic porphyrin concentrations (see Supplementary Materials, Fig. S6), were observed for up to 72 h after the protocols had been carried out. Porphyrin **1** and **2** did not cause a significant reduction in HT-29 cell growth under US exposure (Fig. 6). On the other hand, porphyrin **3** lead to a significant HT-29 cell growth decrease under US exposure after 72 h ($p < 0.01$), whereas porphyrin **4** caused an even more marked HT-29 cell growth decrease at 48 ($p < 0.05$) and 72 h ($p < 0.001$)

(Fig. 6). As observed in Fig. 7, all porphyrins induced a significant reduction in cell proliferation under light irradiation, while porphyrins **3** and **4** showed marked reductions even 48 h ($p < 0.01$) after irradiation. The key role that the sensitiser plays in the sonodynamic process is also highlighted by the sonodynamic effect's dependency on porphyrin dose (see Supplementary Materials, Fig. S7). Moreover, a ROS scavenging assay was carried with NAC to clarify the correlation between intracellular ROS production and the cancer cell death induced by the sonodynamic treatment. Our experiments showed that NAC suppressed cytotoxicity when HT-29 cells were treated with porphyrins and US (see Supplementary Materials, Fig. S8).

It is also worth mentioning that no statistically significant changes in cell proliferation were observed in HDF cells that were incubated with porphyrins and exposed to US (see Supplementary Materials, Fig. S9), whereas HDF cells that were incubated with porphyrins and exposed to light showed the same cytotoxicity pattern as HT-29 cells (Fig. 7).

Cell ROS generation by the sonodynamic and photodynamic activation of porphyrins

A cytofluorimetric evaluation of ROS generation was performed to further confirm whether porphyrin-mediated sonodynamic and photodynamic treatments are able to induce intracellular ROS production.

Differing ROS production patterns were obtained, depending on the porphyrin used, when HT-29 cells underwent US exposure. As shown in Fig. 8, a significant increase in ROS production over time was only observed under US exposure when HT-29 cells were pre-incubated with porphyrin **3** or porphyrin **4,** with a maximum in ROS production being found 30 min after treatment ($p < 0.001$). As seen in Fig. 9, light exposure induced a maximum in ROS production, 30 min after treatment, in HT-29 cells that had previously been incubated with all the porphyrins under consideration ($p < 0.001$). This was followed by a progressive decrease in ROS production up to 60 min after

treatment. In particular, a significant increase in ROS production was observed 1 min after the cells that had previously been incubated with porphyrin **4** were exposed to light ($p < 0.01$).

Overall, it was observed that photodynamic treatment was able to induce a significant increase in ROS production in all the porphyrins under consideration, while sonodynamic treatment was only able to induce a significant increase in ROS production in cells that had previously been incubated with porphyrin **3** or **4**. We can also highlight the fact that the results obtained in the cytofluorimetric ROS evaluations are in line with the effects observed in our cell growth analyses.

Evaluation of cell death via the sonodynamic or photodynamic activation of porphyrins

We decided to focus our attention on the type of cell death induced by sonodynamic porphyrin activation and that we focus our investigation on porphyrin **4**, which showed the highest US-responsiveness. As reported in Table 1, cytofluorimetric cell death analyses were performed 24 h after sonodynamic and photodynamic treatment with porphyrin **4**. Results highlight that sonodynamic treatment induced apoptotic ($19.9 \pm 3.1\%$ of cell population, $p < 0.01$) and necrotic cell death ($19.7 \pm 4.5\%$ of cell population, $p < 0.01$), whereas photodynamic treatment mainly induced necrotic cell death ($39.7 \pm 2.5\%$ of cell population, $p < 0.001$).

Furthermore, TEM analyses were performed 12 h after sonodynamic treatment with porphyrin **4** to also investigate the role of autophagy in sonodynamic ROS-mediated cell death. As shown in Fig. 10, control cells, the untreated cells, were found to be either round or oval with numerous microvilli on the plasma membrane, to contain large nuclei with homogeneous chromatin and to have regularly distributed cell organelles (Fig. 10A). Only moderate and irregular increases in the number of organelles or lipid droplets were observed in cells treated with US (Fig. 10B) or porphyrin **4**. Interestingly, cells that had been pre-incubated with porphyrin **4** and exposed to US showed an abundance of double and single membrane-enclosed vesicles in their cytoplasm. A significant increase in the presence of lipid droplets and cell organelles was also evident (Fig. 10C

and D). This evidence indicates that porphyrin **4**-mediated sonodynamic treatment causes a change in cell metabolism, while an increase in double and single membrane-enclosed vacuoles containing seemingly damaged organelles and digested material indicates the occurrence of autophagy.

DISCUSSION

Porphyrins are excellent sensitisers for ROS production under light irradiation and evidence of their ability to behave as sonosensitisers is slowly accumulating [28, 36, 48]. The aim of this study is to shed light onto the mechanism of ROS formation during the sonodynamic process with porphyrin compounds. 5,10,15,20-tetrakis-(methylpyridinium-4-yl)porphyrin was selected as the sensitiser core structure because of its water solubility and three different metal complexes, namely Fe(III), Zn(II) and Pd(II), were prepared so that we could observe the effects that differing electronic ring properties had on ROS production (efficiency and/or type of ROS produced).

The placing of metals in the porphyrin rings can dramatically alter the spectroscopic behaviour of the chromophore [49]. In particular, metal ions affect the ability of porphyrins to undergo intersystem crossing (ISC) and can also influence the lifetimes of the resulting excited triplets, which in turn modifies the behaviour and the efficiency of the sensitiser [50, 51]. Indeed, free-base porphyrin **1** is moderately efficient in generating singlet oxygen following light irradiation. The insertion of Zn(II) into porphyrin **3,** and Pd(II) into porphyin **4** improves the efficiency of singlet oxygen generation by enhancing ISC and facilitating conversion to the excited triplet state. Pd(II) complexes, in particular, are excellent singlet oxygen generators due to their long triplet lifetime. Moreover, the insertion of Fe(III) into porphyrin **2**, a reportedly poor generator of singlet oxygen, was also chosen as it is known to generate oxygen radicals via single-electron transfer [52]. EPR analyses performed herein confirmed that ROS production following light irradiation was affected by the presence/type of differing metal ion in the porphyrins. Indeed, whereas irradiation with visible light did not lead to the formation of the DMPO/$OH^{\bullet}$ adduct (Fig. 3B) with any of the porphyrins investigated, a signal, which we have attributed to the DMPOX species, was actually observed. This species is formed via the decomposition of the DMPO/$O_2^{\bullet-}$ adduct, as catalysed by low oxidation state metals [47]. The detection of this species suggests the occurrence of one-electron redox reactions, which is expected to be more evident with porphyrin **2**, although the

generation of DMPOX from a reaction between DMPO and singlet oxygen has also been proposed as a possible explanation [53].

In the sonodynamic experiments, while the porphyrins showed different ROS-generating behaviour and efficiency after exposure to non-thermal low intensity US than they did after the light exposure, it must be noted that EPR analyses have demonstrated, for the first time to the best of our knowledge, the sonodynamic generation of hydroxyl radicals and singlet oxygen (Fig. 2A-B). The presence of the DMPO/$OH^{\bullet}$ signal indicates the generation of hydroxyl radical, however the DMPO/$OH^{\bullet}$ species may also results from the decomposition of the unstable adducts of DMPO with superoxide/hydroperoxyl radicals to diamagnetic species and DMPO/$OH^{\bullet}$ [54]. It is worth noting that all porphyrins generate both oxygenated radicals and singlet oxygen, with porphyrin **3** and porphyrin **4** showing the highest efficiency, respectively. Indeed, porphyrin **3** shows the highest signal intensity for the paramagnetic adduct DMPO/$OH^{\bullet}$, whereas porphyrin **4** displays a low intensity signal for the same adduct (Fig. 3A). Porphyrin **4** generates an intense signal for the radical TEMPONE, which is formed from the reaction between singlet oxygen and the probe 4-oxo-TMP (Fig. 3B). Crucially, the absence of signals of oxygenated radicals in the EPR spectra obtained from Ar-saturated solutions of porphyrins **3** and **4** strongly suggests molecular oxygen as the source of US porphyrin-mediated ROS generation.

Taken together, the EPR data show that the efficiency of ROS production is generally lower in SDT than in PDT, however the markedly more efficient ROS-generating behaviour observed for porphyrins **3** and **4** prompted us to investigate whether an US-mediated photo-activation may also underpins SDT.

A number of authors have suggested a quite peculiar US phenomenon, referred to as the emission of light by a mechanical wave, sonoluminescence (SL), to explain the photo-activation mechanism that underlies the production of ROS by SDT. It was therefore decided to perform experiments to investigate the occurrence of SL in our experimental setup. Specifically, SL is the light emission in

the UV-visible range caused by the ionization of noble gases inside the cavitation bubbles, which induces the formation of plasma that in turn ionises the molecules present in the vapour phase within the bubbles, or at the gas-liquid interface of the collapsing bubble [55, 56]. SL can be observed as occurring after stimulation in the ultrasonic frequency range, from 20 kHz up to 3 MHz, and is influenced by variables such as acoustic pressure, frequency, liquid proprieties, temperature and specific gas content [18]. SL emission from clouds of bubbles generated by an ultrasonic transducer is called multi-bubble sonoluminescence (MBSL) [57]. MBSL was investigated in water and in aqueous solutions and in the presence of porphyrins **3** and **4**, which proved the most active in generating ROS upon US exposure in this work. The typical broad band SL emission was observed for all solutions confirmed the occurrence of SL. In particular, SL intensity was markedly more intense in Ar-flushed solution than in air-equilibrated solution. An intriguing feature emerging from our experiments was an emission peak around 310-340 nm observed in the solution of porphyrin **3**, which corresponds to emission of light by hydroxyl radicals, namely OH($A^2\Sigma^+ - X^2\ \Pi_{[1/2,3/2]}$) hydroxyl radical emission. Although the generation of hydroxyl radicals via the homolytic splitting of water was described as occurring during acoustic cavitation several years ago [58], this reaction should be excluded in our system due to the low power of the applied US. Indeed, the absence of oxygenated radicals from the EPR spectra of simple aqueous solutions exposed to US confirms the absence of homolytic water cleavage. Therefore, we conclude that our US experimental setup causes SL emissions in the UV/visible range of the electromagnetic spectrum, both in water and in the presence of porphyrins **3** and **4**. The hydroxyl radical emission observed in the presence of porphyrin 3, supports the hypothesis that SL may play a role in the sonodynamic activation of porphyrins.

We then investigated the biological effects that the same sonodynamic and photodynamic experiments had in an *in vitro* cancer model. The uptake of our porphyrins by HT-29 cancer cells 24 h after incubation was confirmed, as shown by confocal microscopy (Fig. 5), before analyses of

the anticancer effects of sonodynamic and photodynamic activation took place. Upon US exposure, the biological responsiveness of porphyrins **1**-**4** mirrors the results of EPR analyses, as significant cancer cell proliferation inhibition was demonstrated, but only when porphyrin **4** and, to a lesser extent, porphyrin **3** were used as sonosenitizers. The photodynamic activity of porphyrins **1**-**4** also followed the trend observed in the EPR experiments, showing a strong reduction in cancer cell proliferation with all porphyrins tested just 24 h after photodynamic treatment. The pivotal role that the sensitiser plays in the sonodynamic process was confirmed by the fact that the induced cytotoxicity was dependent on porphyrin dose (Fig. S7). In addition, it can be stated that sonodynamic cytotoxicity was mainly ascribable to porphyrin-mediated ROS production (Fig. S8), as the ROS scavenger, NAC, prevented HT-29 cell death.

DCF fluorescence, measured after our sono- and photodynamic cell treatments, was observed as a redox imbalance indicator, rather than a direct measure of intracellular H_2O_2, since DCFH-DA is the most widely used probe for detecting hydroxyl radical and other highly reactive oxygen species, then the oxidative stress [59]. The DCFH-DA assay was therefore performed to provide an indirect evaluation of intracellular ROS generation after cells that had been pre-incubated with porphyrin **1**-**4** where exposed to either US or light. Interestingly, common timings were observed upon comparing sonodynamic and photodynamic intracellular ROS production (Fig. 8 and 9); the highest values were observed 30 min after US and light exposure, but to differing extents depending on the trigger (US or light) and the intracellular porphyrin complex (**1**-**4**) used. While porphyrins **3** and **4** were found to be the most effective at generating intracellular ROS upon US exposure, all the porphyrins were able to efficiently generate ROS upon light exposure. These data support the hypothesis that the possible mechanism of action for effective sonodynamic anticancer response derives from the ROS elicited by the US activation of the sensitiser, such as in the well-clinically established PDT technique where cancer cell killing is achieved through oxidative stress. We thus

feel, as do other authors [60-62], that sonodynamic treatment deserves further investigation for its potential as an intriguing strategy for cancer treatment.

Another important aspect is the fact that PDT leads to cell death via multiple pathways. Indeed, oxidative stress mediates apoptotic and/or necrotic cell death, but also induces autophagy, which can cause the overconsumption of the cellular machinery necessary for maintaining cellular vitality when excessive. This results in type-II programmed cell death (PCD), which is better known as "autophagic cell death" (ACD). Apoptosis and autophagic cell death can occur simultaneously and excessive autophagy can also regulate the apoptotic pathway [63, 64], which underpins the importance of cross-talk between autophagy and apoptosis when ROS are among the main intracellular signal transducers that sustain cancer cell death. Moreover, antioxidant treatment prevents autophagy, suggesting that redox imbalance plays a pivotal role in driving the process. To further confirm that oxidative stress was at the basis of sonodynamic killing of cance cells in our experimental considtions, we investigated the cell death as induced by the porphyrin with the highest US-responsiveness, porphyrin **4.** Whereas the porphyrin **4** sonodynamiyc ROS-mediated process induced both necrotic and apoptotic cell death, light exposure was responsible for necrotic cell death (Table 1). These data are in agreement with the ROS analyses carried out using EPR and a DCF-DA assay. In fact, the higher extent of necrotic cell death that was observed upon photodynamic treatment may be due to the higher singlet oxygen production and redox imbalance that it causes, as compared to sonodynamic treatment. Moreover, TEM observation of cells under sonodynamic treatment with porphyrin **4** were carried out to investigate the possible occurrence of ACD and cells with significantly increased numbers of autophagosomes were observed, giving them the characteristic vacuolated appearance, that is peculiar to ACD. The extensive ROS production achieved upon the exposure of porphyrin **4** to US is therefore able to switch the autophagic defence response against oxidative stress into a lethal stimulus that leads to ACD.

The data reported here point out the importance of sensitiser properties when attempting to achieve US-induced ROS generation that can lead to cancer cell death. Indeed, the different patterns of ROS generation depend on the presence and type of the metal in the macrocycle; porphrin **4** is the most efficient in generating singlet oxygen, hydroxyl radicals and, consequently, causing cancer cell death under US exposure.

It is worth noting that the sonodynamic treatment of the human dermal fibroblast cell line HDF did not produce any significant effect on cell proliferation, suggesting that also the different cell membrane properties can be crucial to the outcome and selectivity of the sonodynamic treatment, unlike what observed with the photodynamic treatment (Fig. S9). Indeed, it is well known that cancer and non-cancerous cells can display wildly different cell structure and mechanical properties, including membrane stiffness, membrane permeability and cellular adhesion [65-67]. For instance, early stage investigations have demonstrated the existence of a relathionship bewteen cell elastic properties and US bioeffects [68, 69]. This remark can be supported by an intriguing hypothesis introduced by Krasovitski and colleagues [70], in which non-thermal US induces bilayer membrane motion that can help elucidate the mechanisms of US interaction with biological tissue that are currently not fully understood. In their work, the authors presented an intracellular cavitation mechanism to explain some US biological effects, from delicate and reversible bioeffects [71], to complete membrane disruption and irreversible cellular damage [72]. Moreover, in a previous work, we ourselves have shown that the cavitation zone passes through a number of stages of evolution and SL seems to develop accordingly [27]. In this scenario, it is not unreasonable to assume that the intracellular cavitation mechanism might also elicit an intracellular cavitation zone with different stages of evolution that are able to trigger our porphyrin compounds.

In conclusion, the present work demonstrates, for the first time, that the sonodynamic efficacy of porphyrins in cancer cell killing can vary according to the metal moiety present in the macrocycle, seemingly because it is responsible for different ROS generation patterns. Finally, we are providing

ex cellulo evidence suggesting that porphyrin activation by US can be mediated by photo-activation *via* sonoluminescence rather than a radical path process *via* homolytic splitting of water.

Author contributions

L.S. and R.C. designed the study; F.G., F.F., A.M.M., A.T. and A.P. performed research; L.S. R.C. and I.F. contributed to data analysis and interpretation; N.V.D. and G.D. drafted the article and critically revised it; F.G., L.S. and R.C. wrote the paper.

Competing financial interests

The authors declare that no competing financial interests exist

Acknowledgment

The Authors gratefully acknowledge funding from the Associazione Italiana per la Ricerca sul Cancro (AIRC, grant "MFAG 2012", MFAG-13048) and from the University of Torino (grant "Ricerca Locale 2015"). We are grateful to Prof. Maria Teresa Capucchio for carrying out TEM analyses and to Dr. Vanessa Pinnelli for assistance with *in vitro* cell experiments.

REFERENCES

[1] D. Costley, C. Mc Ewan, C. Fowley, A.P. McHale, J. Atchison, N. Nomikou, J.F. Callan, Treating cancer with sonodynamic therapy: a review, Int J Hyperthermia 31(2) (2015) 107-17.

[2] L. Serpe, F. Giuntini, Sonodynamic antimicrobial chemotherapy: First steps towards a sound approach for microbe inactivation, J Photochem Photobiol B 150 (2015) 44-9.

[3] Y. Li, Q. Zhou, Z. Deng, M. Pan, X. Liu, J. Wu, F. Yan, H. Zheng, IR-780 Dye as a Sonosensitizer for Sonodynamic Therapy of Breast Tumor, Sci Rep 6 (2016) 25968.

[4] J. Cheng, X. Sun, S. Guo, W. Cao, H. Chen, Y. Jin, B. Li, Q. Li, H. Wang, Z. Wang, Q. Zhou, P. Wang, Z. Zhang, W. Cao, Y. Tian, Effects of 5-aminolevulinic acid-mediated sonodynamic therapy on macrophages, Int J Nanomedicine 8 (2013) 669-76.

[5] D.G. You, V.G. Deepagan, W. Um, S. Jeon, S. Son, H. Chang, H.I. Yoon, Y.W. Cho, M. Swierczewska, S. Lee, M.G. Pomper, I.C. Kwon, K. Kim, J.H. Park, ROS-generating TiO2 nanoparticles for non-invasive sonodynamic therapy of cancer, Sci Rep 6 (2016) 23200.

[6] C. Brazzale, R. Canaparo, L. Racca, F. Foglietta, G. Durando, R. Fantozzi, P. Caliceti, S. Salmaso, L. Serpe, Enhanced selective sonosensitizing efficacy of ultrasound-based anticancer treatment by targeted gold nanoparticles, Nanomedicine (Lond) 11(23) (2016) 3053-3070.

[7] G. Varchi, F. Foglietta, R. Canaparo, M. Ballestri, F. Arena, G. Sotgiu, A. Guerrini, C. Nanni, G. Cicoria, G. Cravotto, S. Fanti, L. Serpe, Engineered porphyrin loaded core-shell nanoparticles for selective sonodynamic anticancer treatment, Nanomedicine (Lond) 10(23) (2015) 3483-94.

[8] V.G. Deepagan, D.G. You, W. Um, H. Ko, S. Kwon, K.Y. Choi, G.R. Yi, J.Y. Lee, D.S. Lee, K. Kim, I.C. Kwon, J.H. Park, Long-Circulating Au-TiO2 Nanocomposite as a Sonosensitizer for ROS-Mediated Eradication of Cancer, Nano Lett (2016).

[9] P. Huang, X. Qian, Y. Chen, L. Yu, H. Lin, L. Wang, Y. Zhu, J. Shi, Metalloporphyrin-Encapsulated Biodegradable Nanosystems for Highly Efficient Magnetic Resonance Imaging-Guided Sonodynamic Cancer Therapy, J Am Chem Soc 139(3) (2017) 1275-1284.

[10] Y. Lv, J. Zheng, Q. Zhou, L. Jia, C. Wang, N. Liu, H. Zhao, H. Ji, B. Li, W. Cao, Antiproliferative and Apoptosis-inducing Effect of exo-Protoporphyrin IX based Sonodynamic Therapy on Human Oral Squamous Cell Carcinoma, Sci Rep 7 (2017) 40967.

[11] G. ter Haar, Heat and sound: focused ultrasound in the clinic, Int J Hyperthermia 31(3) (2015) 223-4.

[12] I. Lentacker, I. De Cock, R. Deckers, S.C. De Smedt, C.T. Moonen, Understanding ultrasound induced sonoporation: definitions and underlying mechanisms, Adv Drug Deliv Rev 72 (2014) 49-64.

[13] W.D. O'Brien, Jr., Ultrasound-biophysics mechanisms, Prog Biophys Mol Biol 93(1-3) (2007) 212-55.

[14] A.P. McHale, J.F. Callan, N. Nomikou, C. Fowley, B. Callan, Sonodynamic Therapy: Concept, Mechanism and Application to Cancer Treatment, Adv Exp Med Biol 880 (2016) 429-50.

[15] G.Y. Wan, Y. Liu, B.W. Chen, Y.Y. Liu, Y.S. Wang, N. Zhang, Recent advances of sonodynamic therapy in cancer treatment, Cancer Biol Med 13(3) (2016) 325-338.

[16] W.L. Nyborg, Biological effects of ultrasound: development of safety guidelines. Part II: general review, Ultrasound Med Biol 27(3) (2001) 301-33.

[17] T.G. Leighton, What is ultrasound?, Prog Biophys Mol Biol 93(1-3) (2007) 3-83.

[18] K.S. Suslick, D.J. Flannigan, Inside a collapsing bubble: sonoluminescence and the conditions during cavitation, Annu Rev Phys Chem 59 (2008) 659-83.

[19] M. Kohno, T. Mokudai, T. Ozawa, Y. Niwano, Free radical formation from sonolysis of water in the presence of different gases, J Clin Biochem Nutr 49(2) (2011) 96-101.

[20] Y. Matsumura, A. Iwasawa, T. Kobayashi, T. Kamachi, T. Ozawa, M. Kohno, Detection of High-frequency Ultrasound-induced Singlet Oxygen by the ESR Spin-trapping Method, Chem Lett 42(10) (2013) 1291-1293.

[21] A. Miyaji, M. Kohno, Y. Inoue, T. Baba, Hydroxyl radical generation by dissociation of water molecules during 1.65 MHz frequency ultrasound irradiation under aerobic conditions, Biochem Biophys Res Commun 483(1) (2017) 178-182.

[22] M. Dular, B. Bachert, S. B., B. Širok, Relationship between cavitation structures and cavitation damage, Wear 257(11) (2004) 8.

[23] Y.T. Didenko, K.S. Suslick, The energy efficiency of formation of photons, radicals and ions during single-bubble cavitation, Nature 418(6896) (2002) 394-7.

[24] R. Pflieger, T. Chave, M. Virot, S.I. Nikitenko, Activating molecules, ions, and solid particles with acoustic cavitation, J Vis Exp (86) (2014).

[25] L.A. Crum, Resource Paper: Sonoluminescence, J Acoust Soc Am 138(4) (2015) 2181-205.

[26] N.V. Dezhkunov, A. Francescutto, P. Ciuti, T.J. Mason, G. Iernetti, A.I. Kulak, Enhancement of sonoluminescence emission from a multibubble cavitation zone, Ultrason Sonochem 7(1) (2000) 19-24.

[27] N.V. Dezhkunov, A. Francescutto, L. Serpe, R. Canaparo, G. Cravotto, Sonoluminescence and acoustic emission spectra at different stages of cavitation zone development, Ultrason Sonochem (2017).

[28] A. Sazgarnia, A. Shanei, H. Eshghi, M. Hassanzadeh-Khayyat, H. Esmaily, M.M. Shanei, Detection of sonoluminescence signals in a gel phantom in the presence of Protoporphyrin IX conjugated to gold nanoparticles, Ultrasonics 53(1) (2013) 29-35.

[29] S. Umemura, N. Yumita, R. Nishigaki, K. Umemura, Mechanism of cell damage by ultrasound in combination with hematoporphyrin, Jpn J Cancer Res 81(9) (1990) 962-6.

[30] C. McEwan, H. Nesbitt, D. Nicholas, O.N. Kavanagh, K. McKenna, P. Loan, I.G. Jack, A.P. McHale, J.F. Callan, Comparing the efficacy of photodynamic and sonodynamic therapy in non-melanoma and melanoma skin cancer, Bioorg Med Chem 24(13) (2016) 3023-8.

[31] Y. Shimamura, D. Tamatani, S. Kuniyasu, Y. Mizuki, T. Suzuki, H. Katsura, H. Yamada, Y. Endo, T. Osaki, M. Ishizuka, T. Tanaka, N. Yamanaka, T. Kurahashi, Y. Uto, 5-Aminolevulinic Acid Enhances Ultrasound-mediated Antitumor Activity via Mitochondrial Oxidative Damage in Breast Cancer, Anticancer Res 36(7) (2016) 3607-12.

[32] Y. Li, Q. Zhou, Z. Hu, B. Yang, Q. Li, J. Wang, J. Zheng, W. Cao, 5-Aminolevulinic Acid-Based Sonodynamic Therapy Induces the Apoptosis of Osteosarcoma in Mice, PLoS One 10(7) (2015) e0132074.

[33] Z. Hu, H. Fan, G. Lv, Q. Zhou, B. Yang, J. Zheng, W. Cao, 5-Aminolevulinic acid-mediated sonodynamic therapy induces anti-tumor effects in malignant melanoma via p53-miR-34a-Sirt1 axis, J Dermatol Sci 79(2) (2015) 155-62.

[34] W. Hiraoka, H. Honda, L.B. Feril, Jr., N. Kudo, T. Kondo, Comparison between sonodynamic effect and photodynamic effect with photosensitizers on free radical formation and cell killing, Ultrason Sonochem 13(6) (2006) 535-42.

[35] I. Rosenthal, J.Z. Sostaric, P. Riesz, Sonodynamic therapy--a review of the synergistic effects of drugs and ultrasound, Ultrason Sonochem 11(6) (2004) 349-63.

[36] H. Chen, X. Zhou, Y. Gao, B. Zheng, F. Tang, J. Huang, Recent progress in development of new sonosensitizers for sonodynamic cancer therapy, Drug Discov Today 19(4) (2014) 502-9.

[37] R.F. Pasternack, E.J. Gibbs, A. Gaudemer, A. Antebi, S. Bassner, L. De Poy, D.H. Turner, A. Williams, F. Laplace, M.H. Lansard, C. Merienne, M. Perree-Fauvet, Molecular complexes of nucleosides and nucleotides with a monomeric cationic porphyrin and some of its metal derivatives, J Am Chem Soc 107(26) (1985) 8179-8186.

[38] P.G.W.P. Harriman A, Photo-oxidation of metalloporphyrins in aqueous solution, J Chem Soc Faraday Trans 1 79 (1983) 21.

[39] B. Zeqiri, C.J. Bickley, A new anechoic material for medical ultrasonic applications, Ultrasound Med Biol 26(3) (2000) 481-5.

[40] A. Troia, D. Madonna Ripa, Sonoluminescence in liquid metals, J Phys Chem C 117(11) (2013) 6.

[41] A.A. Ndiaye, R. Pflieger, B. Siboulet, J. Molina, J.F. Dufreche, S.I. Nikitenko, Nonequilibrium vibrational excitation of OH radicals generated during multibubble cavitation in water, J Phys Chem A 116(20) (2012) 4860-7.

[42] X. Wang, H. Fang, Z. Huang, W. Shang, T. Hou, A. Cheng, H. Cheng, Imaging ROS signaling in cells and animals, J Mol Med (Berl) 91(8) (2013) 917-27.

[43] S. Mrakic-Sposta, M. Gussoni, M. Montorsi, S. Porcelli, A. Vezzoli, Assessment of a standardized ROS production profile in humans by electron paramagnetic resonance, Oxid Med Cell Longev 2012 (2012) 973927.

[44] R. Konaka, E. Kasahara, W.C. Dunlap, Y. Yamamoto, K.C. Chien, M. Inoue, Irradiation of titanium dioxide generates both singlet oxygen and superoxide anion, Free Radic Biol Med 27(3-4) (1999) 294-300.

[45] I. Fenoglio, J. Ponti, E. Alloa, M. Ghiazza, I. Corazzari, R. Capomaccio, D. Rembges, S. Oliaro-Bosso, F. Rossi, Singlet oxygen plays a key role in the toxicity and DNA damage caused by nanometric TiO2 in human keratinocytes, Nanoscale 5(14) (2013) 6567-76.

[46] M. Ghiazza, E. Alloa, S. Oliaro-Bosso, F. Viola, S. Livraghi, D. Rembges, R. Capomaccio, F. Rossi, J. Ponti, I. Fenoglio, Inhibition of the ROS-mediated cytotoxicity and genotoxicity of nano-TiO2 toward human keratinocyte cells by iron doping, J Nanopart Res 16(2) (2014).

[47] E. Finkelstein, G.M. Rosen, E.J. Rauckman, Spin trapping of superoxide and hydroxyl radical: practical aspects, Arch Biochem Biophys 200(1) (1980) 1-16.

[48] Q. Liu, X. Wang, P. Wang, L. Xiao, Sonodynamic antitumor effect of protoporphyrin IX disodium salt on S180 solid tumor, Chemotherapy 53(6) (2007) 429-36.

[49] T. Ohse, S. Nagaoka, Y. Arakawa, H. Kawakami, K. Nakamura, Cell death by reactive oxygen species generated from water-soluble cationic metalloporphyrins as superoxide dismutase mimics, J Inorg Biochem 85(2-3) (2001) 201-8.

[50] A. Harriman, Luminescence of porphyrins and metalloporphyrins. Part 1. -Zinc(II), nickel(II) and manganese(II) porphyrins, J Chem Soc Faraday Trans 1 76 (1980) 8.

[51] A. Harriman, Luminescence of porphyrins and metalloporphyrins. Part 2.-Copper(II), chromium(III), manganese(III), iron(II) and iron(III) porphyrins, J Chem Soc Faraday Trans 1 77 (1981) 9.

[52] B. Meunier, Metalloporphyrins as versatile catalysts for oxidation reactions and oxidative DNA cleavag, Chem Rev 92(6) (1992) 16.

[53] R.K. Bilski P, Bilska M & Chignell CF, Oxidation of the Spin Trap 5,5-Dimethyl-1-pyrroline N-Oxide by Singlet Oxygen in Aqueous Solution, J Am Chem Soc 118(6) (1996) 9.

[54] E. Finkelstein, G.M. Rosen, E.J. Rauckman, Production of hydroxyl radical by decomposition of superoxide spin-trapped adducts, Mol Pharmacol 21(2) (1982) 262-5.

[55] N. Garcia, A.P. Levanyuk, V.V. Osipov, Nature of sonoluminescence: noble gas radiation excited by hot electrons in cold water, Phys Rev E Stat Phys Plasmas Fluids Relat Interdiscip Topics 62(2 Pt A) (2000) 2168-76.

[56] K.S. Suslick, S.J. Doktycz, E.B. Flint, On the origin of sonoluminescence and sonochemistry, Ultrasonics 28(5) (1990) 280-90.

[57] Y.T. Didenko, T.V. Gordeychuk, Multibubble sonoluminescence spectra of water which resemble single-bubble sonoluminescence, Phys Rev Lett 84(24) (2000) 5640-3.

[58] M.W. Didenko YT, Suslick KS, Temperature of Multibubble Sonoluminescence in Water, J Phys Chem A 103(50) (1999) 6.

[59] B. Kalyanaraman, V. Darley-Usmar, K.J. Davies, P.A. Dennery, H.J. Forman, M.B. Grisham, G.E. Mann, K. Moore, L.J. Roberts, 2nd, H. Ischiropoulos, Measuring reactive oxygen and nitrogen species with fluorescent probes: challenges and limitations, Free Radic Biol Med 52(1) (2012) 1-6.

[60] H. Hirschberg, S.J. Madsen, Synergistic efficacy of ultrasound, sonosensitizers and chemotherapy: a review, Ther Deliv 8(5) (2017) 331-342.

[61] M. Trendowski, The promise of sonodynamic therapy, Cancer Metastasis Rev 33(1) (2014) 143-60.

[62] A.K. Wood, C.M. Sehgal, A review of low-intensity ultrasound for cancer therapy, Ultrasound Med Biol 41(4) (2015) 905-28.

[63] G. Filomeni, D. De Zio, F. Cecconi, Oxidative stress and autophagy: the clash between damage and metabolic needs, Cell Death Differ 22(3) (2015) 377-88.

[64] V. Inguscio, E. Panzarini, L. Dini, Autophagy Contributes to the Death/Survival Balance in Cancer PhotoDynamic Therapy, Cells 1(3) (2012) 464-91.

[65] H.H. Lin, H.K. Lin, I.H. Lin, Y.W. Chiou, H.W. Chen, C.Y. Liu, H.I. Harn, W.T. Chiu, Y.K. Wang, M.R. Shen, M.J. Tang, Mechanical phenotype of cancer cells: cell softening and loss of stiffness sensing, Oncotarget 6(25) (2015) 20946-58.

[66] H. Liu, Q. Tan, W.R. Geddie, M.A. Jewett, N. Phillips, D. Ke, C.A. Simmons, Y. Sun, Biophysical characterization of bladder cancer cells with different metastatic potential, Cell Biochem Biophys 68(2) (2014) 241-6.

[67] V. Swaminathan, K. Mythreye, E.T. O'Brien, A. Berchuck, G.C. Blobe, R. Superfine, Mechanical stiffness grades metastatic potential in patient tumor cells and in cancer cell lines, Cancer Res 71(15) (2011) 5075-80.

[68] X. Chen, R.S. Leow, Y. Hu, J.M. Wan, A.C. Yu, Single-site sonoporation disrupts actin cytoskeleton organization, J R Soc Interface 11(95) (2014) 20140071.

[69] A. Geltmeier, B. Rinner, D. Bade, K. Meditz, R. Witt, U. Bicker, C. Bludszuweit-Philipp, P. Maier, Characterization of Dynamic Behaviour of MCF7 and MCF10A Cells in Ultrasonic Field Using Modal and Harmonic Analyses, PLoS One 10(8) (2015) e0134999.

[70] B. Krasovitski, V. Frenkel, S. Shoham, E. Kimmel, Intramembrane cavitation as a unifying mechanism for ultrasound-induced bioeffects, Proc Natl Acad Sci U S A 108(8) (2011) 3258-63.

[71] W.J. Tyler, Y. Tufail, M. Finsterwald, M.L. Tauchmann, E.J. Olson, C. Majestic, Remote excitation of neuronal circuits using low-intensity, low-frequency ultrasound, PLoS One 3(10) (2008) e3511.

[72] D. Dalecki, Mechanical bioeffects of ultrasound, Annu Rev Biomed Eng 6 (2004) 229-48.

Table 1 Cell death analysis 24 h after treatment

HT-29 cells	Live cells	Apoptotic cells	Necrotic cells
Untreated cells	95.2 ± 8.3	2.5 ± 0.9	2.3 ± 0.6
Light	94.9 ± 9.2	4.1 ± 1.0	0.9 ± 0.2
US	95.0 ± 7.3	3.2 ± 0.7	1.8 ± 0.5
4	95.4 ± 8.4	4.0 ± 0.6	0.6 ± 0.1
4 + Light	53.3 ± 4.5 ***	7.0 ±0.9	39.7 ± 2.5 ***
4 + US	60.4 ± 5.8 ***	19.9 ± 3.1 **	19.7 ± 4.5 **

Statistical significance *vs* untreated cells: ** $p < 0.01$, *** $p < 0.001$.

FIGURE LEGENDS

Fig. 1 Structures of porphyrins **1**-**4**

Fig. 2 Generation of hydroxyl radicals (A) and of singlet oxygen (B) by the various porphyrins (**1**-**4**) following activation by US power at 1.5 W/cm^2 for 5 min at 1.866 MHz, as detected by EPR spectroscopy. Signal intensity is proportional to the amount of reactive species generated.

Fig. 3 Generation of hydroxyl radicals (A) and of singlet oxygen (B) by the various porphyrins (**1**-**4**) following activation by light power at 51.8 mW/cm^2 for 5 min at 400-1050 nm, as detected by EPR spectroscopy. Signal intensity is proportional to the amount of reactive species generated.

Fig. 4 Sonoluminescence emission spectra of porphyrin **3** (black curve) and **4** (red curve) solutions under air saturation during US irradiation at 1.5 W/cm^2 for 5 min, at 1.866 MHz. The blue curve refers to multi bubble sonoluminescence (MBSL) recorded in aqueous solution, while the grey curve corresponds to the background of the acquiring system.

Fig. 5 Representative confocal fluorescence images of HT-29 cells incubated with the various porphyrins. Cells were exposed to either 500 μM of porphyrin **1**, **2** or **4** or 250 μM of porphyrin **3** (green) for 24 h; TO-PRO®-3 (blue) was used a nuclear counterstain. Magnification: 40x. Scale bars: 15 μm.

Fig. 6 Effects of sonodynamic treatment on HT-29 cell growth. HT-29 cells were incubated for 24 h with the various porphyrins (**1**, **2** and **4** at 500 μM; **3** at 250 μM) and then exposed to US power at 1.5 W/cm^2 for 5 min at 1.866 MHz. Cell proliferation was evaluated after 24, 48 and 72 h using the WST-1 assay. Statistically significant difference *versus* untreated cells: * $p < 0.05$, ** $p < 0.01$.

Fig. 7 Effects of photodynamic treatment on HT-29 cell growth. HT-29 cells were incubated for 24 h with the various porphyrins (**1**, **2** and **4** at 500 μM; **3** at 250 μM) and then exposed to light power at 51.8 mW/cm^2 for 5 min at 400-1050 nm. Cell proliferation was evaluated after 24, 48 and 72 h using the WST-1 assay. Statistically significant difference v*ersus* untreated cells: * $p < 0.05$, ** $p < 0.01$, *** $p < 0.001$.

Fig. 8 HT-29 reactive oxygen species production after sonodynamic treatment. HT-29 cells were exposed to US (1.5 W/cm^2 for 5 min at 1.866 MHz) either alone or after 24 h incubation with the various porphyrins (**1**, **2** and **4** at 500 μM; **3** at 250 μM). ROS levels were determined according to the 2',7'-dichlorofluorescein diacetate (DCF-DA) assay using flow cytometry and expressed as the integrated average fluorescence ratio (iMFI) ratio, as described in Materials and Methods. Statistically significant difference *versus* untreated cells (represented by a dashed lines): * $p < 0.05$, ** $p < 0.01$, *** $p < 0.001$.

Fig. 9 HT-29 reactive oxygen species production after photodynamic treatment. HT-29 cells were exposed to light (51.8 mW/cm^2 for 5 min at 400-1050 nm), either alone or after cell incubation for 24 h with the various porphyrins (**1**, **2** and **4** at 500 μM; **3** at 250 μM). ROS levels were determined according to the 2',7'-dichlorofluorescein diacetate (DCF-DA) assay using flow cytometry and expressed as the integrated average fluorescence ratio (iMFI) ratio, as described in Materials and Methods. Statistically significant difference *versus* untreated cells (represented by a dashed lines): * $p < 0.05$, ** $p < 0.01$, *** $p < 0.001$.

Fig. 10 Representative TEM images of HT-29 cells after sonodynamic treatment with porphyrin **4**. Untreated cells (A, 7,500x), cells only exposed to US (1.5 W/cm^2 for 5 min at 1.866 MHz; B, 7,500x) and cells 12 h after sonodynamic treatment with porhyrin **4** having been pre-incubated for

24 h at 500 μM (C, 6,000x; D, 12,000x) are displayed. Vesicles that contained residual digested material or cellular content are indicated by arrows and lipid droplets by stars.

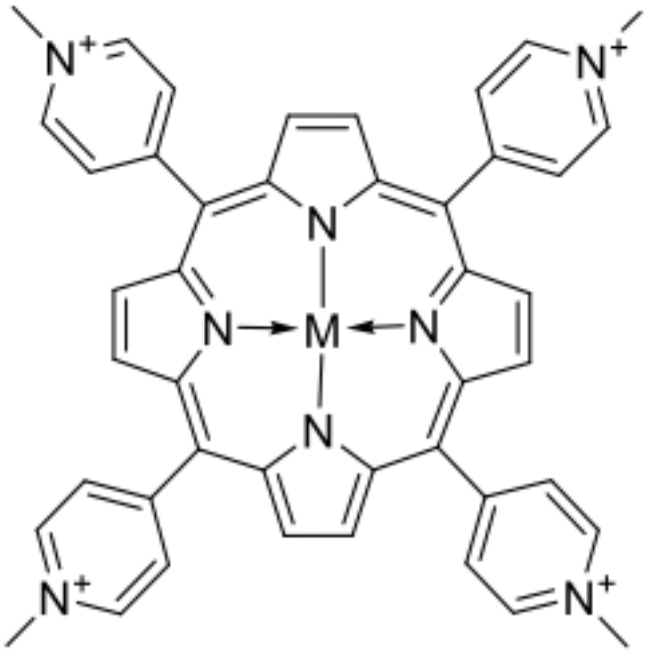

1: M = $2H^+$ **2**: M = $Fe^{3+}(Cl)$

3: M = Zn^{2+} **4**: M = Pd^{2+}

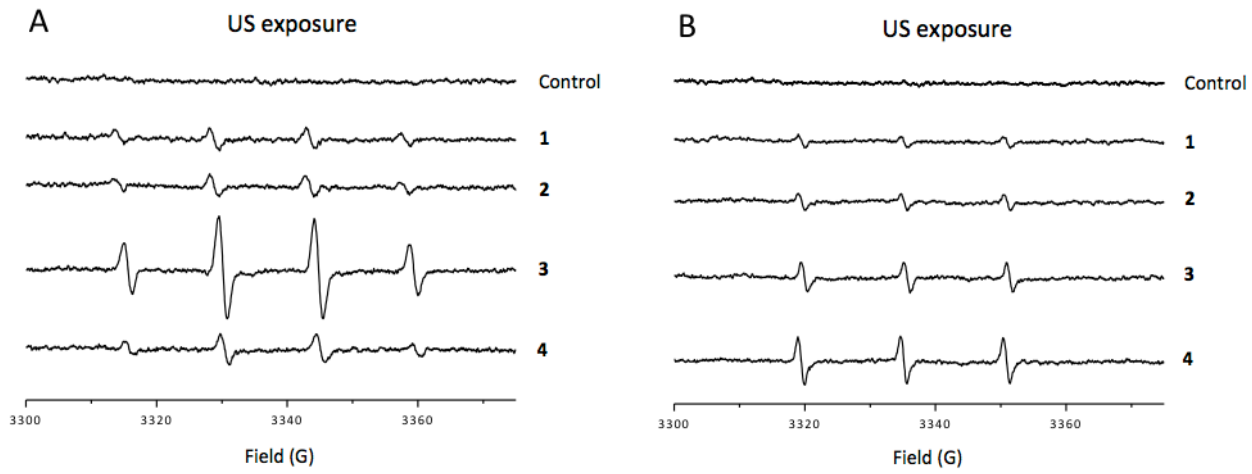
A
US exposure
Control
1
2
3
4
3300
3320
3340
3360
Field (G)
B
US exposure
Control
1
2
3
4
3300
3320
3340
3360
Field (G)

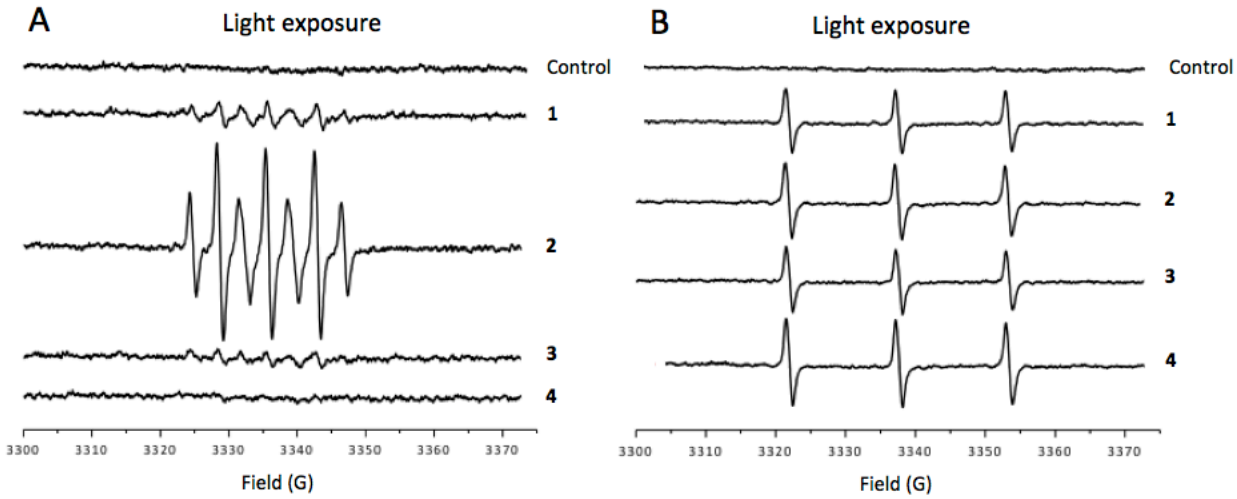
A
Light exposure
Control
1
2
3
4
3300
3310
3320
3330
3340
3350
3360
3370
Field (G)
B
Light exposure
Control
1
2
3
4
3300
3310
3320
3330
3340
3350
3360
3370
Field (G)

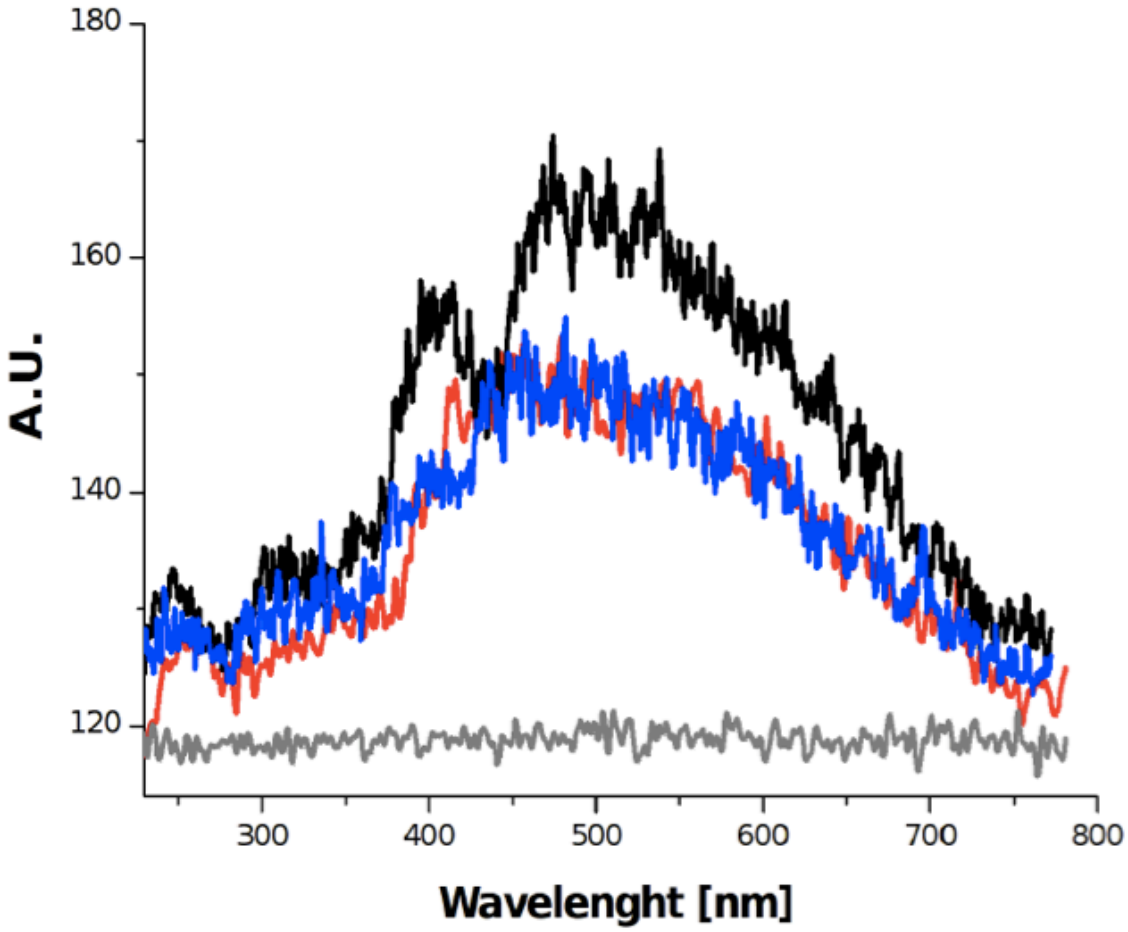
180
160
140
120
A.U.
300
400
500
600
700
800
Wavelenght [nm]

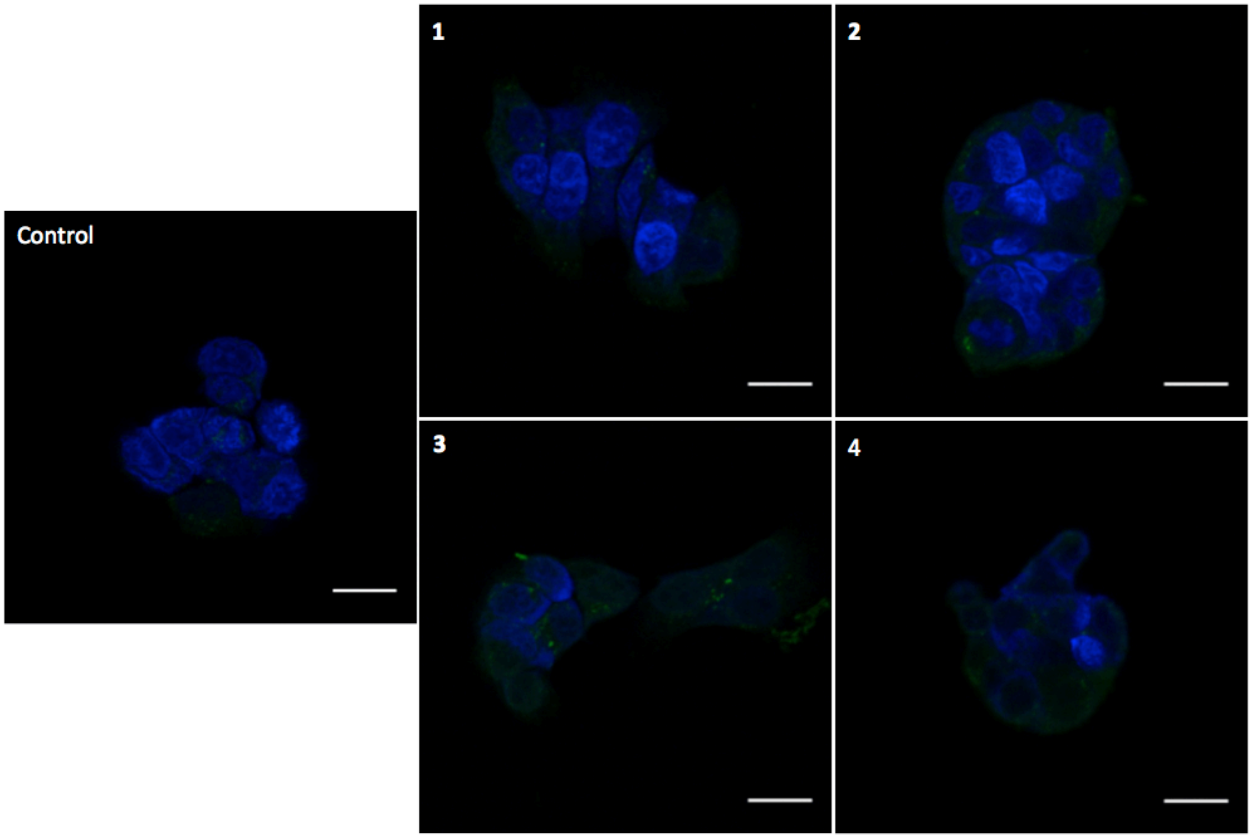
Control
1
2
3
4

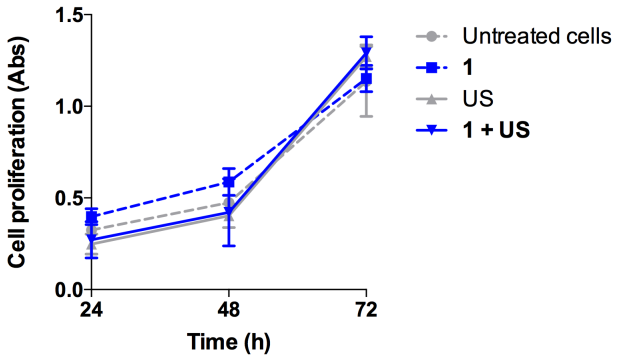
Cell proliferation (Abs)
1.5
1.0
0.5
0.0
24
48
72
Time (h)
Untreated cells
1
US
1 + US

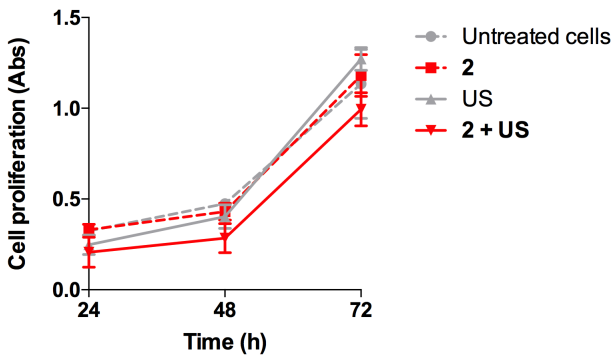
Cell proliferation (Abs)
1.5
1.0
0.5
0.0
24
48
72
Time (h)
Untreated cells
2
US
2 + US

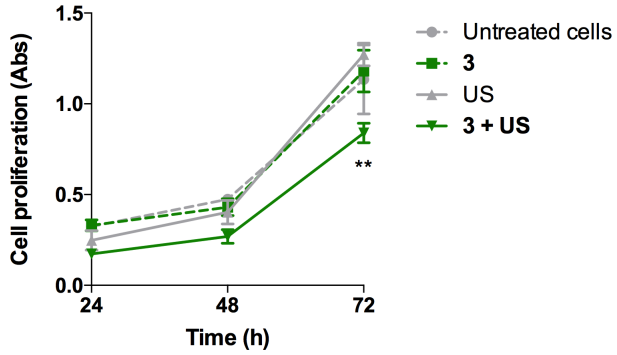
Cell proliferation (Abs)
1.5
1.0
0.5
0.0
24
48
72
Time (h)
**
Untreated cells
3
US
3 + US

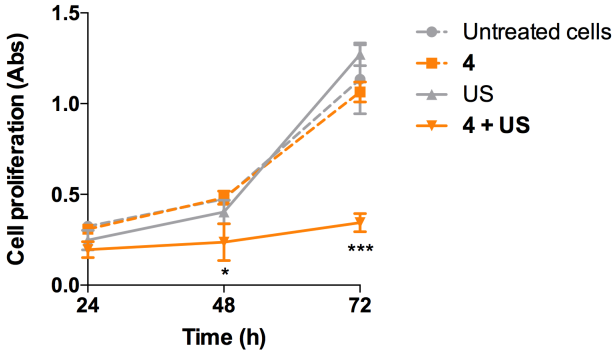
Cell proliferation (Abs)
1.5
1.0
0.5
0.0
24
48
72
Time (h)
*
***
Untreated cells
4
US
4 + US

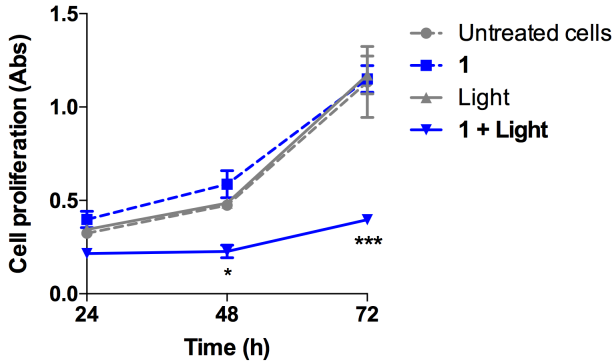
Cell proliferation (Abs)
1.5
1.0
0.5
0.0
24
48
72
Time (h)
*
***
Untreated cells
1
Light
1 + Light

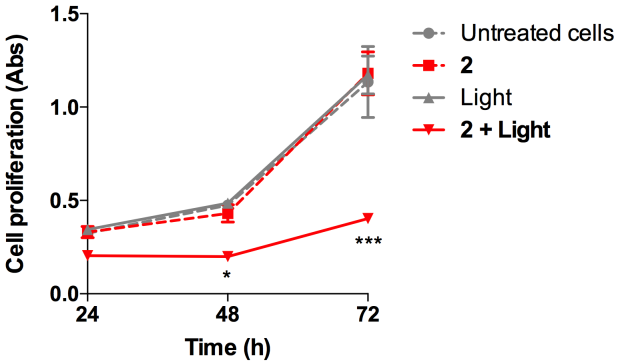
Cell proliferation (Abs)
1.5
1.0
0.5
0.0
24
48
72
Time (h)
*
***
Untreated cells
2
Light
2 + Light

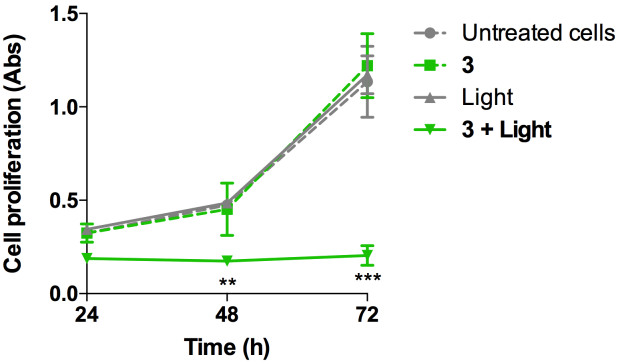
Cell proliferation (Abs)
1.5
1.0
0.5
0.0
24
48
72
Time (h)
**
***
Untreated cells
3
Light
3 + Light

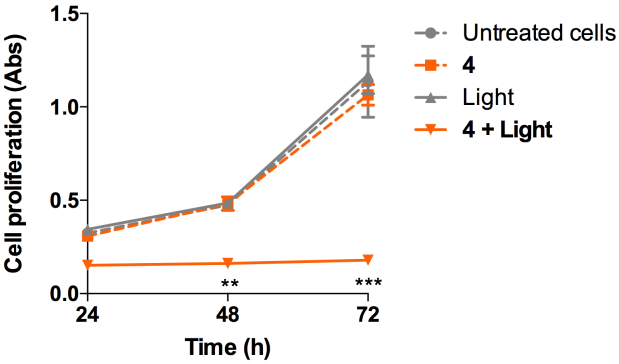
Cell proliferation (Abs)
1.5
1.0
0.5
0.0
24
48
72
Time (h)
**
***
Untreated cells
4
Light
4 + Light

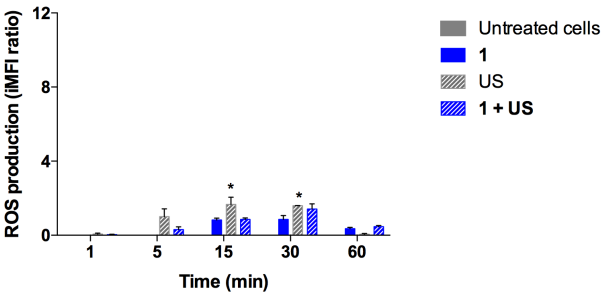
ROS production (iMFI ratio)
12
8
4
0
1
5
15
30
60
Time (min)
Untreated cells
1
US
1 + US

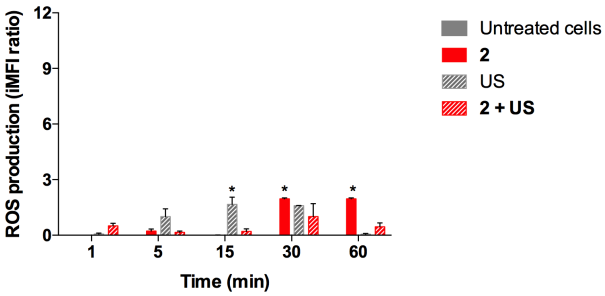
ROS production (iMFI ratio)
12
9
6
3
0
1
5
15
30
60
Time (min)
Untreated cells
2
US
2 + US

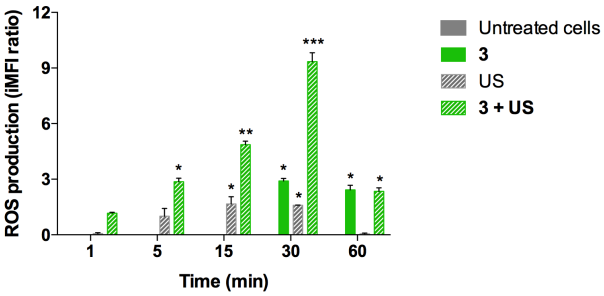
ROS production (iMFI ratio)
12
9
6
3
0
1
5
15
30
60
Time (min)
Untreated cells
3
US
3 + US

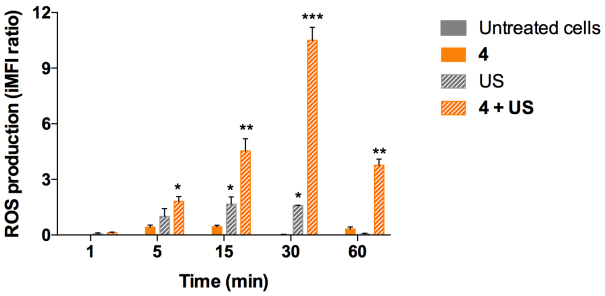
ROS production (iMFI ratio)
12
9
6
3
0
1
5
15
30
60
Time (min)
Untreated cells
4
US
4 + US

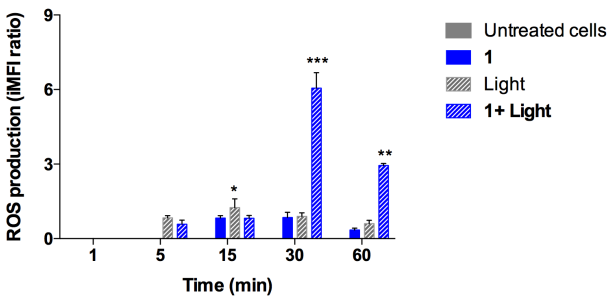
ROS production (iMFI ratio)
9
6
3
0
1
5
15
30
60
Time (min)
***
*
**
Untreated cells
1
Light
1+ Light

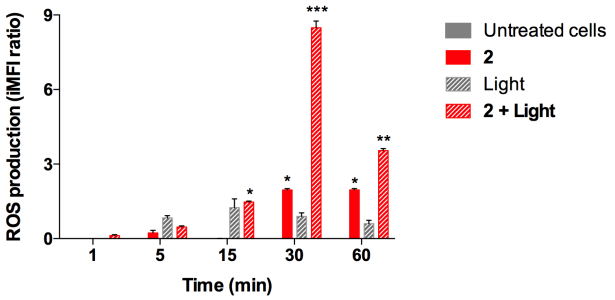
ROS production (iMFI ratio)
9
6
3
0
1
5
15
30
60
Time (min)
***
*
*
*
**
Untreated cells
2
Light
2 + Light

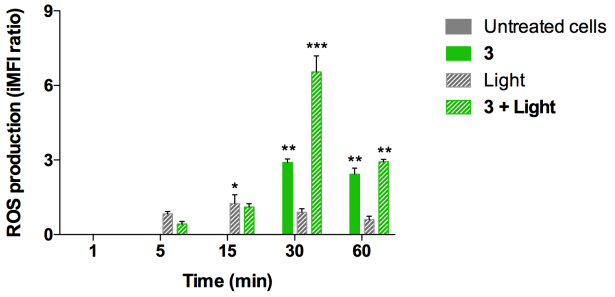
ROS production (iMFI ratio)
9
6
3
0
1
5
15
30
60
Time (min)
***
*
**
**
**
Untreated cells
3
Light
3 + Light

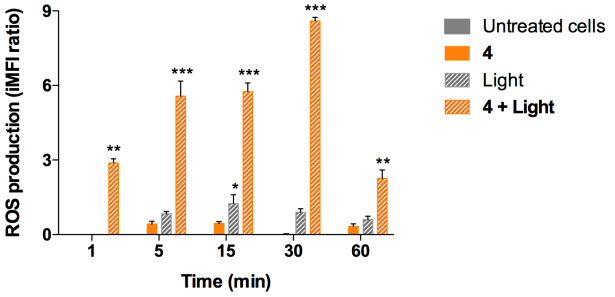
ROS production (iMFI ratio)
9
6
3
0
1
5
15
30
60
Time (min)
***
***
***
*
**
**
Untreated cells
4
Light
4 + Light

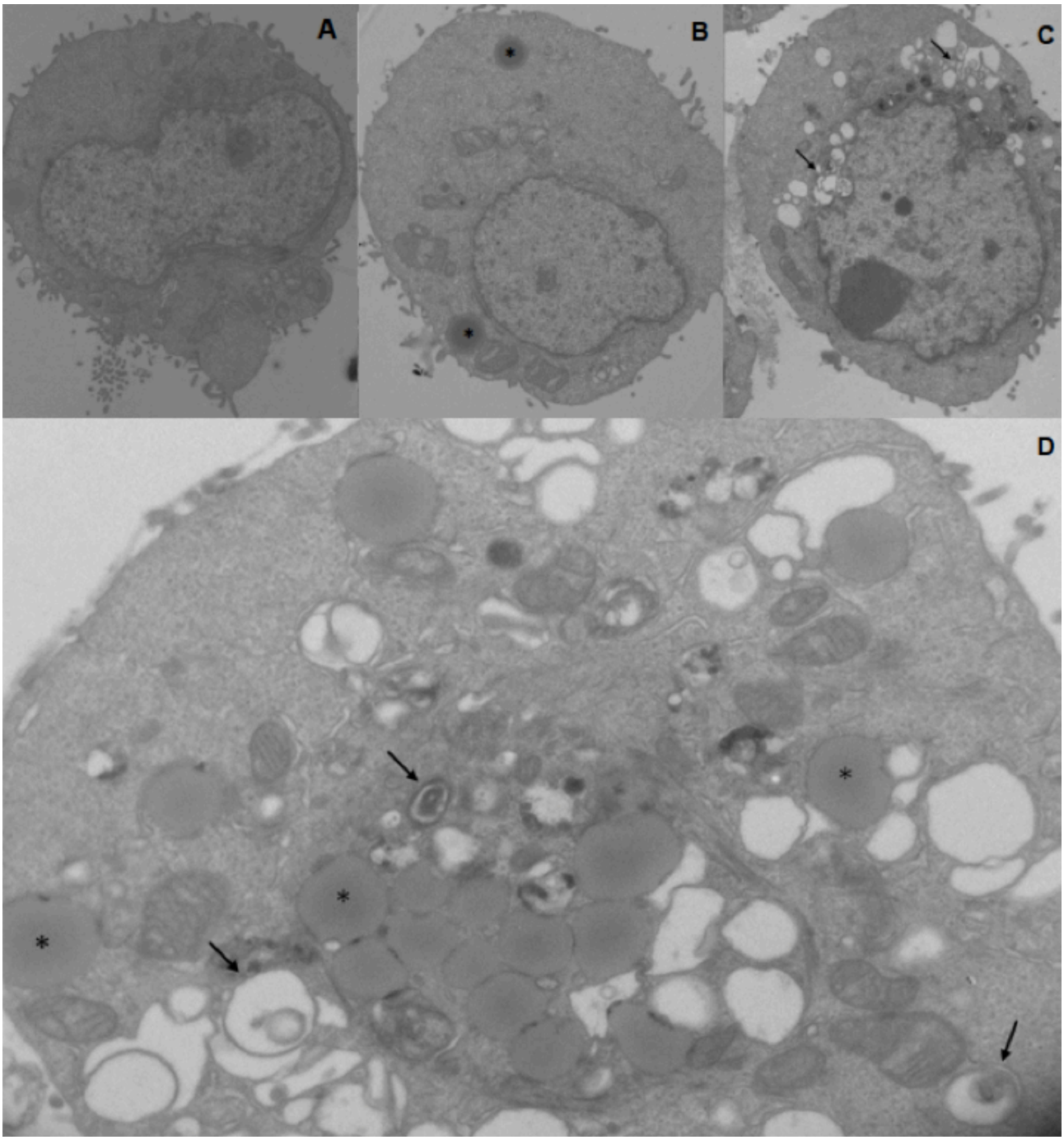
A
B
C
D

SUPPLEMENTARY MATERIALS

Fig. S1 NMR spectra of porphyrin **1** (A), **3** (B) and **4** (C).

Fig. S2 Generation of A) hydroxyl radicals and B) of singlet oxygen by the various porphyrins (**1**-**4**) detected by EPR spectroscopy in the absence of activation.

Fig. S3 Generation of hydroxyl radicals by porphyrin **3** in solution (A) and in the same solution by bubbling Ar in a controlled atmosphere to remove dissolved oxygen for the duration of US exposure (B).

Fig. S4 Simulation of the EPR spectra 2 of Fig. 3A. Splitting constants, A^H: 3.9 G, A^H: 3.9 G; A^N 7.1 G.

Fig. S5 Sonoluminescence emission spectra of air-equilibrated porphyrin **3** (black curve) and **4** (red curve) solutions flushed with Ar during US exposure at 1.5 W/cm^2 for 5 min, at 1.866 MHz. The blue curve refers to multi-bubble sonoluminescence (MBSL) recorded in aqueous solution, while the grey curve corresponds to the background of the acquiring system. The emission around 310-340 nm (*) overlaps somewhat with the broad continuum emission, but is still visible and corresponds to the OH($A^2\Sigma^+ - X^2\,\Pi_{[1/2,3/2]}$) radical emission caused by vibrational bands.

Fig. S6 Effects of porphyrins on HT-29 cell growth. HT-29 cells were incubated for 24 h with increasing concentration of porphyrin **1, 2, 3** and **4** (125, 250, 500 and 1000 μM). Cell proliferation was evaluated after 24 h by WST-1 assay. Statistically significant difference *versus* untreated cells: ** $p < 0.01$ and *** $p < 0.001$.

Fig. S7 Effects of sonodynamic treatment on HT-29 cells as a function of sonosensitiser dose. HT-29 cells were incubated for 24 h with increasing concentration of porphyrin **3** (31.25, 62.50, 125.00 and 250.00 μM) and **4** (62.50, 125.00, 250.00 and 500.00 μM)**,** and then exposed to US power at 1.5 W/cm^2 for 5 min at 1.866 MHz. Cell proliferation was evaluated after 24, 48 and 72 h by WST-1 assay. Statistically significant difference *versus* untreated cells: * $p < 0.05$, ** $p < 0.01$ and *** $p < 0.001$.

Fig. S8 Effects of sonodynamic treatment on HT-29 cells in presence of the ROS scavenger, N-acetyl-cysteine (NAC). HT-29 cells were incubated for 24 h with porphyrin **3** at 250 μM and **4** at 500 μM, and 5.0 mM NAC was added for the last 3 h of porphyrins incubation. Cells were then exposed to US power at 1.5 W/cm^2 for 5 min at 1.866 MHz. Cell proliferation was evaluated after 24, 48 and 72 h by WST-1 assay.

Fig. S9 Effects of sonodynamic and photodynamic treatment on HDF cell growth. HDF cells were incubated for 24 h with porphyrin **3** at 250 μM and **4** at 500 μM, and then exposed to US power at 1.5 W/cm^2 for 5 min at 1.866 MHz and light power at 51.8 mW/cm^2 for 5 min at 400-1050 nm. Cell proliferation was evaluated after 24, 48 and 72 h by WST-1 assay. Statistically significant difference *versus* untreated cells: * $p < 0.05$, *** $p < 0.001$.

A

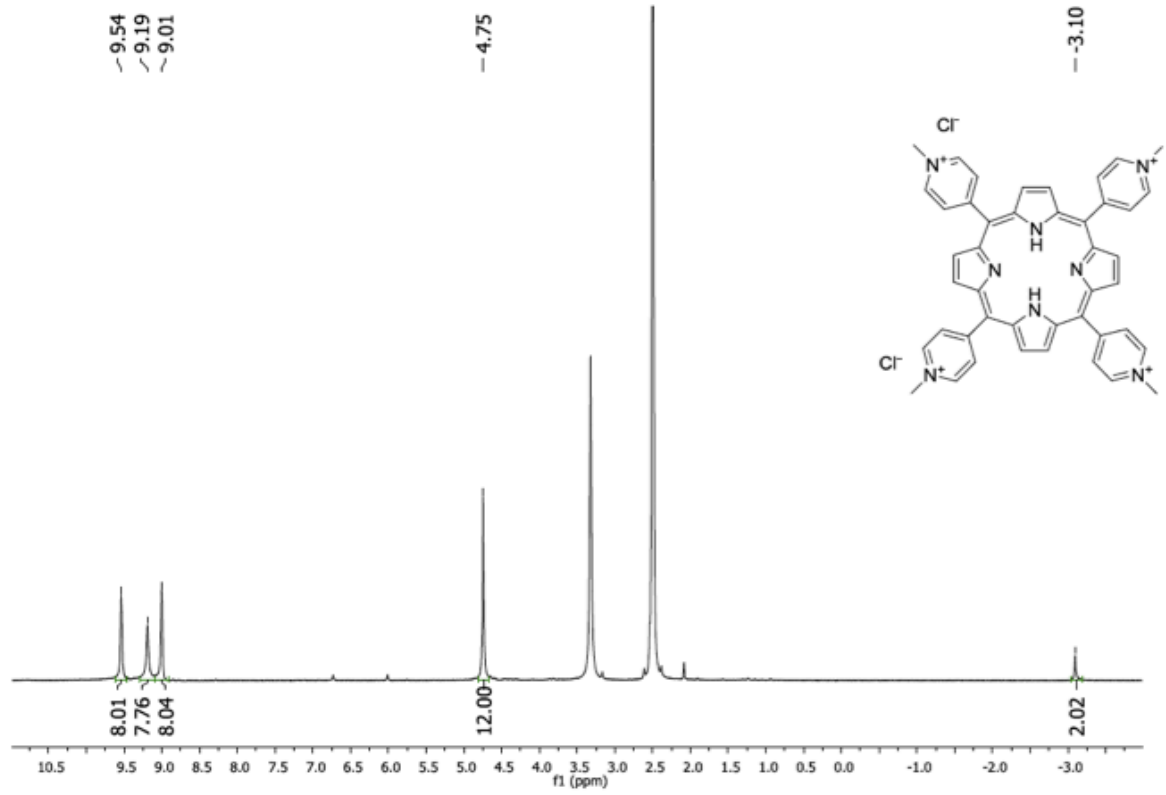
9.54
9.19
9.01
4.75
-3.10
Cl⁻
Cl⁻
8.01
7.76
8.04
12.00
2.02
f1 (ppm)

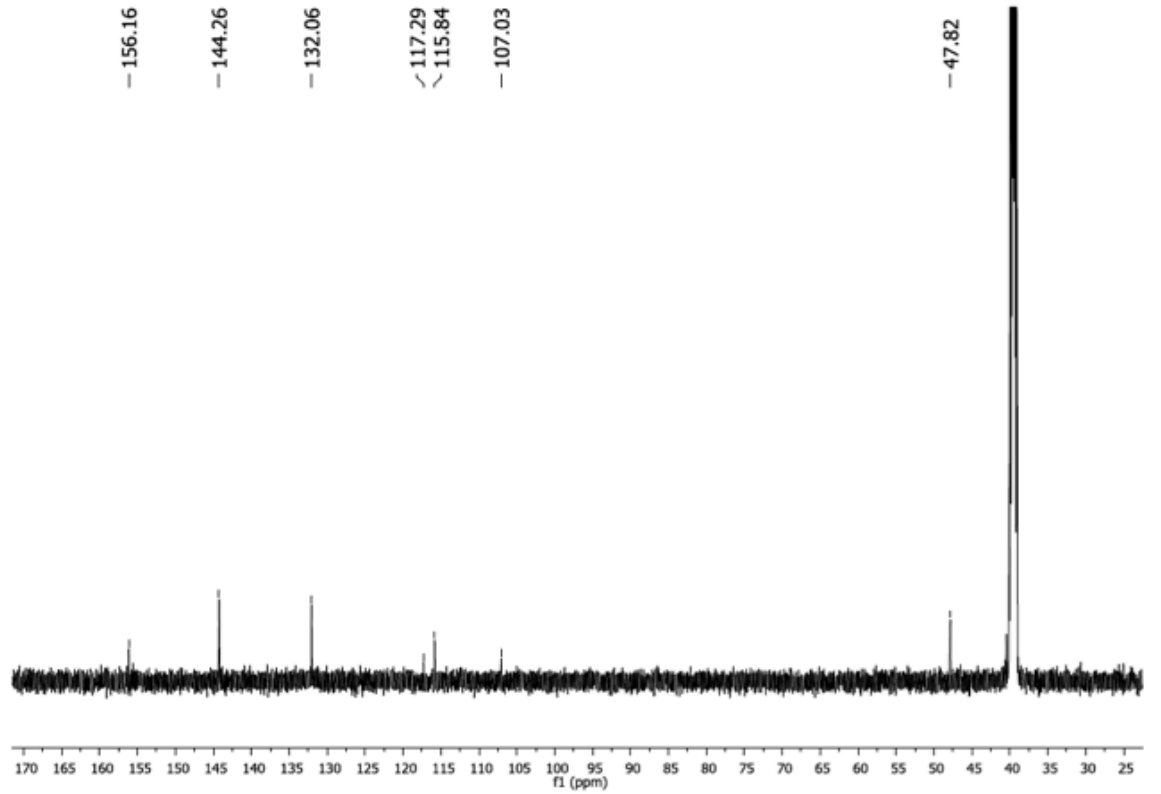
156.16
144.26
132.06
117.29
115.84
107.03
47.82
f1 (ppm)

B

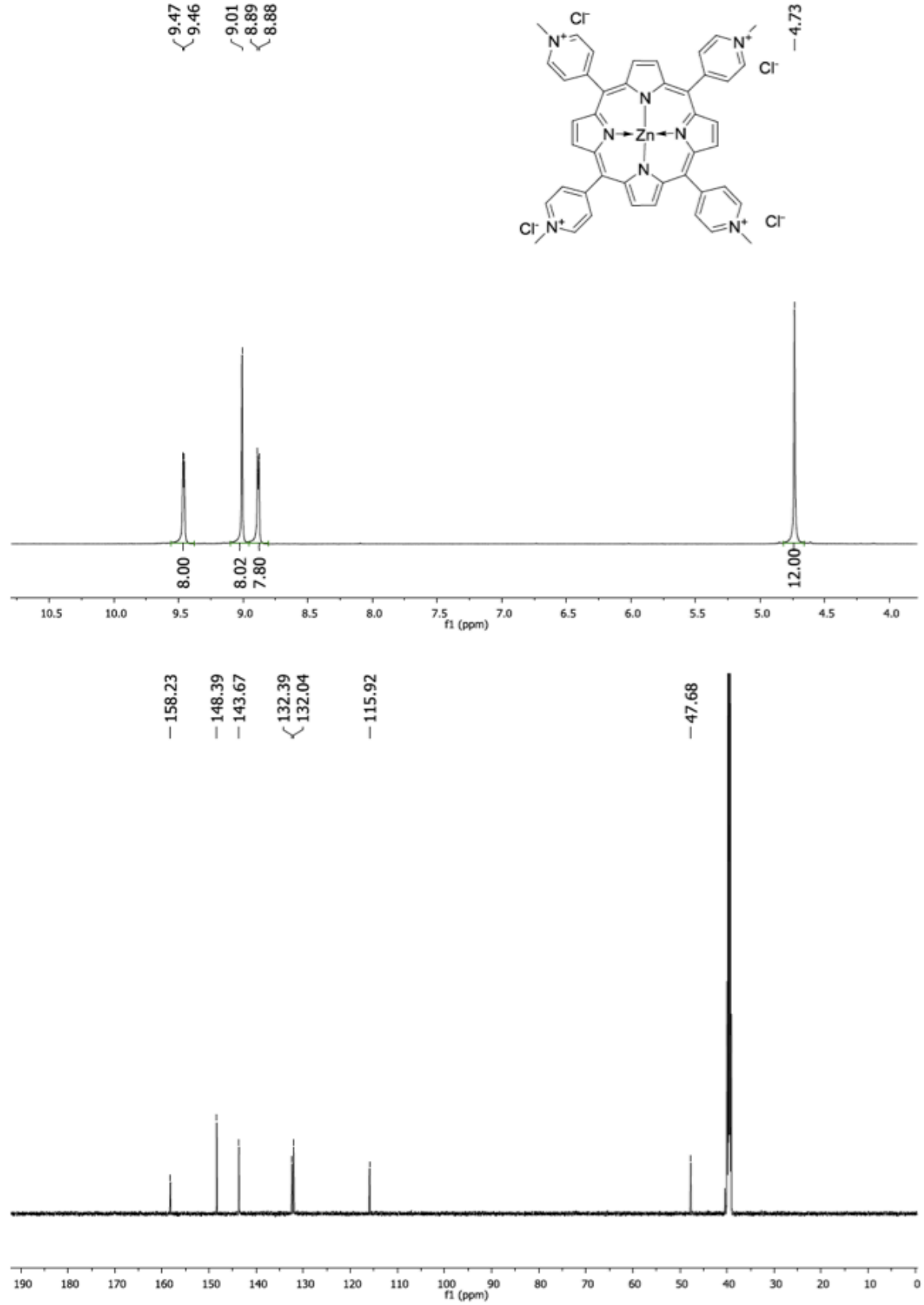
9.47
9.46
9.01
8.89
8.88
4.73
Cl⁻
N⁺
N
Zn
8.00
8.02
7.80
12.00
f1 (ppm)
158.23
148.39
143.67
132.39
132.04
115.92
47.68
f1 (ppm)

C

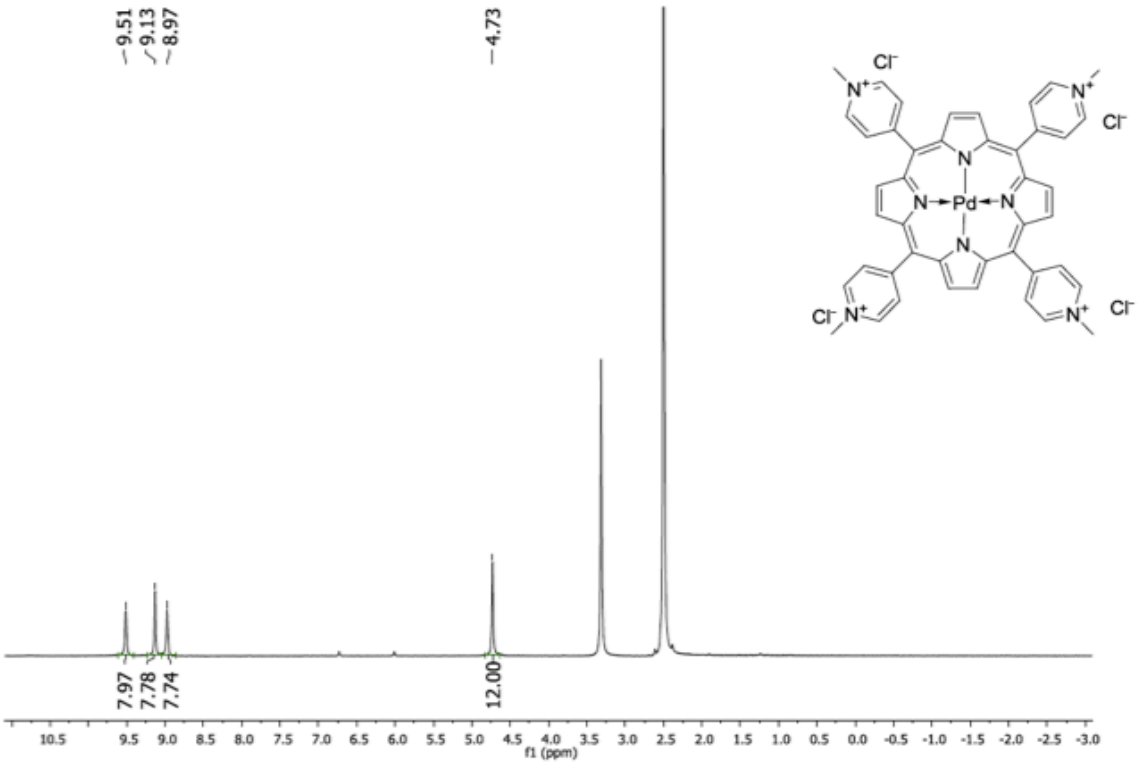
9.51
9.13
8.97
4.73
7.97
7.78
7.74
12.00
Cl⁻
N⁺
N
Pd
f1 (ppm)

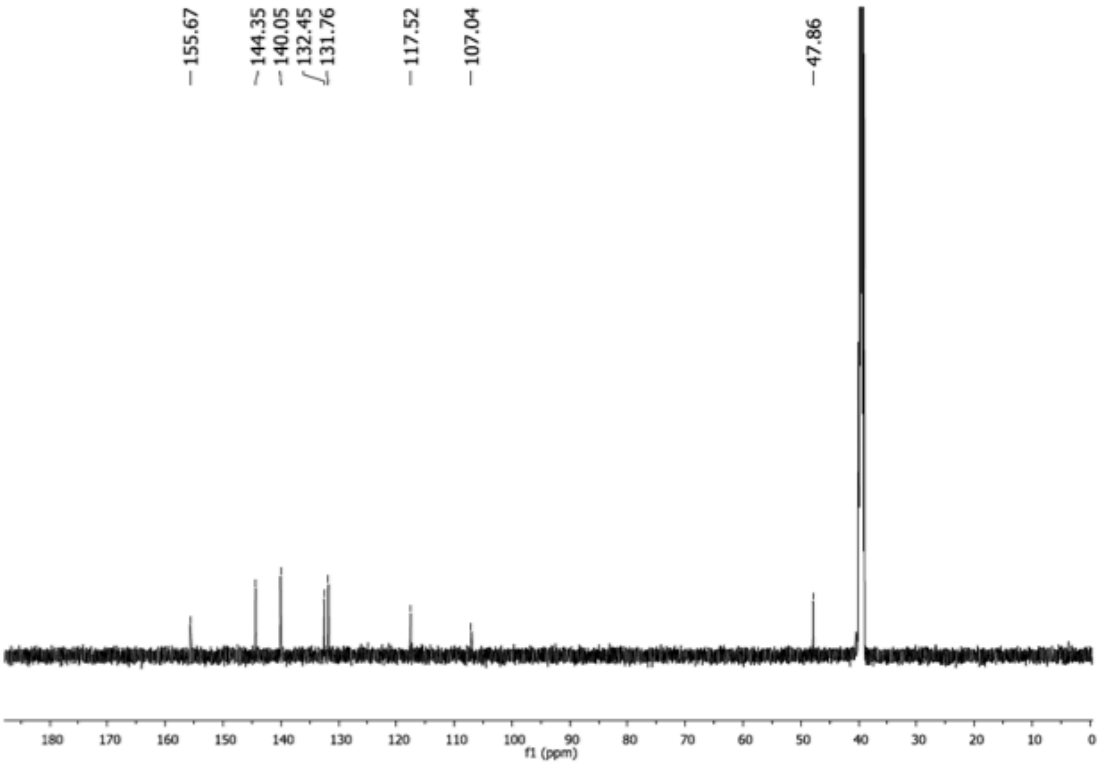
155.67
144.35
140.05
132.45
131.76
117.52
107.04
47.86
f1 (ppm)

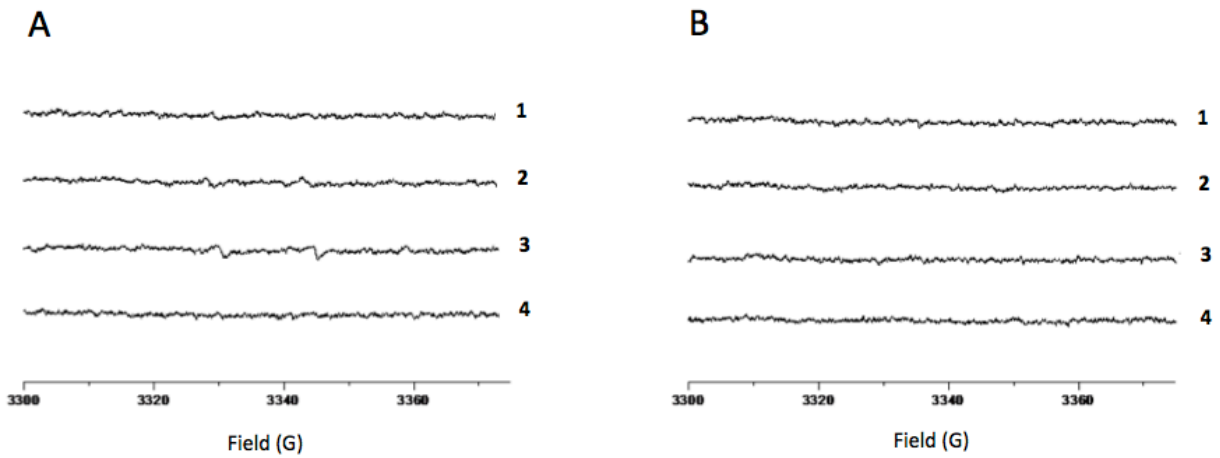
A
1
2
3
4
3300
3320
3340
3360
Field (G)
B
1
2
3
4
3300
3320
3340
3360
Field (G)

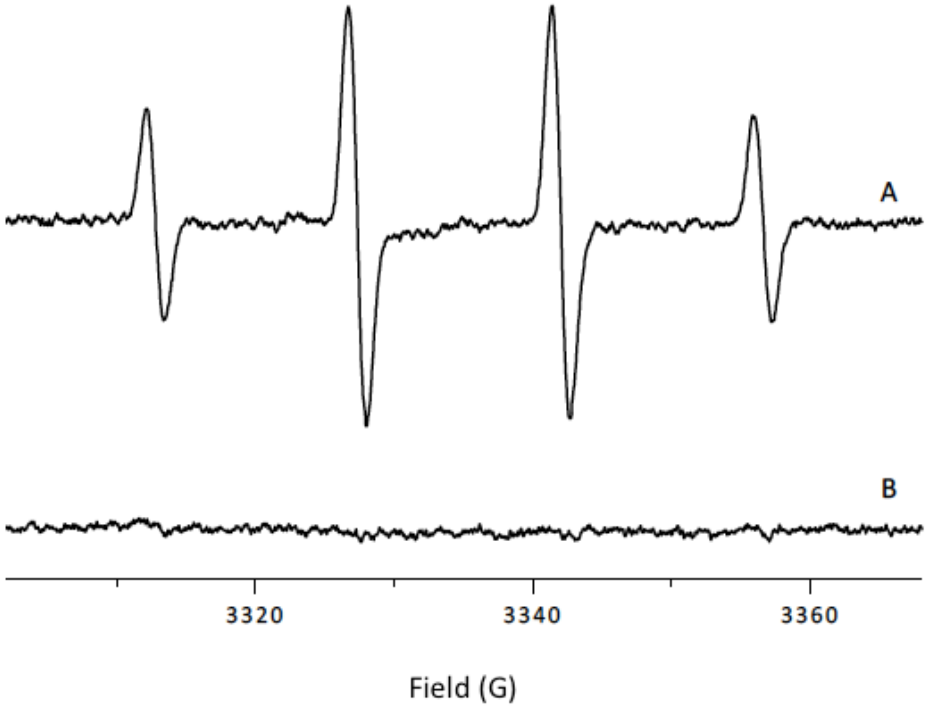
A
B
3320
3340
3360
Field (G)

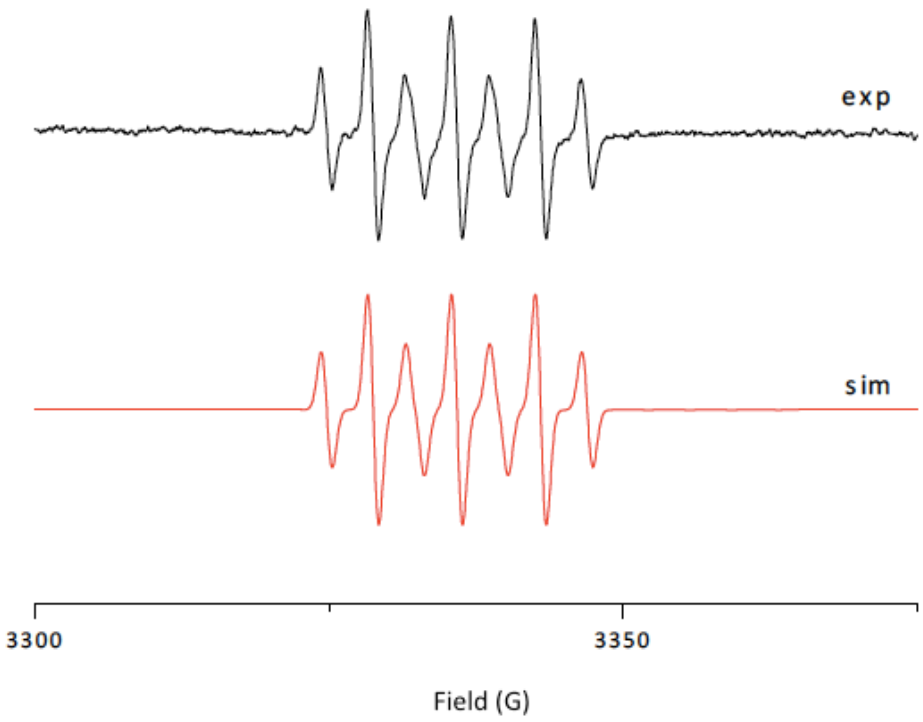
exp
sim
3300
3350
Field (G)

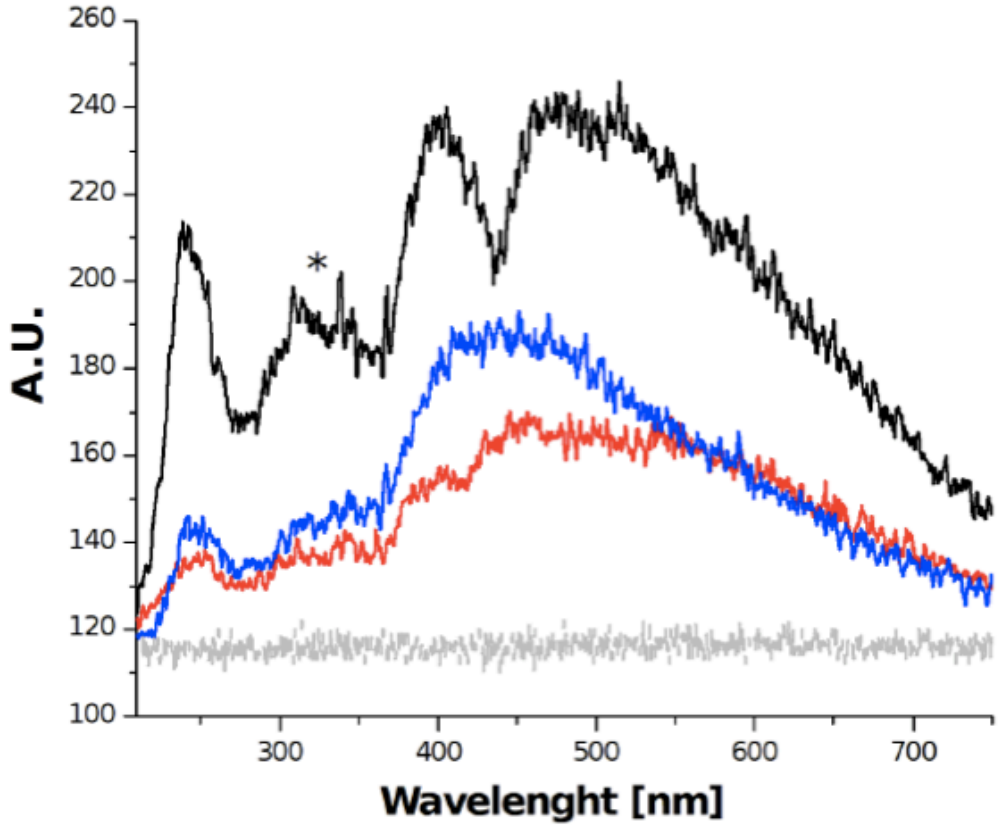
260
240
220
200
180
160
140
120
100
A.U.
*
300
400
500
600
700
Wavelenght [nm]

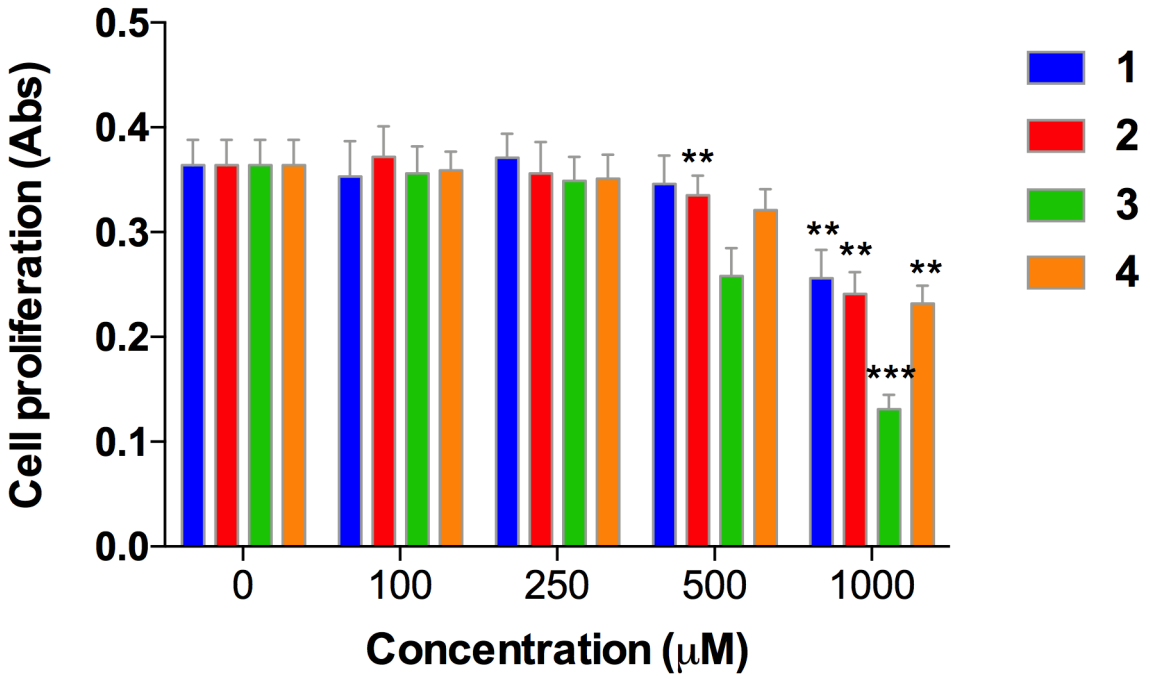
Cell proliferation (Abs)
0.5
0.4
0.3
0.2
0.1
0.0
0
100
250
500
1000
Concentration (μM)
**
**
**
***
**
1
2
3
4

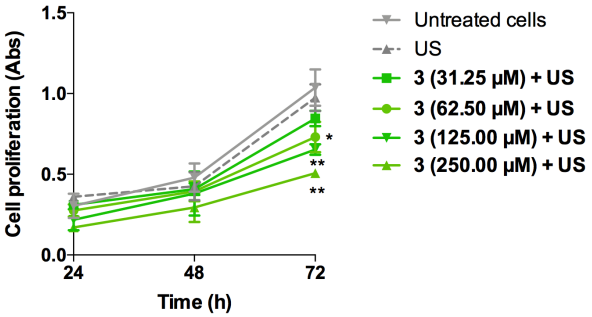
Cell proliferation (Abs)
1.5
1.0
0.5
0.0
24
48
72
Time (h)
*
**
**
Untreated cells
US
3 (31.25 µM) + US
3 (62.50 µM) + US
3 (125.00 µM) + US
3 (250.00 µM) + US

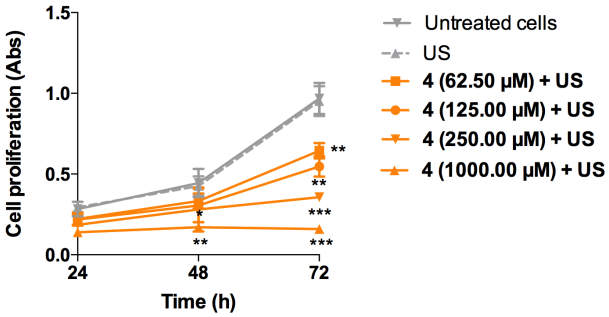
Cell proliferation (Abs)
1.5
1.0
0.5
0.0
24
48
72
Time (h)
**
**
*
**
***
**
***
Untreated cells
US
4 (62.50 µM) + US
4 (125.00 µM) + US
4 (250.00 µM) + US
4 (1000.00 µM) + US

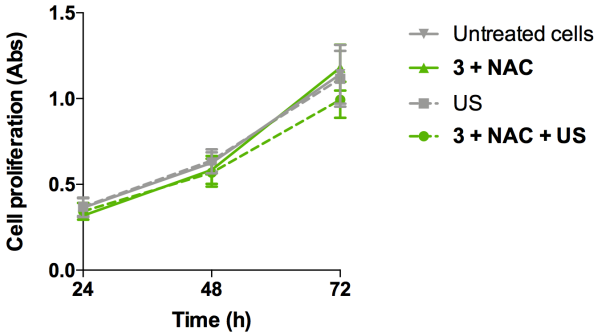
Cell proliferation (Abs)
1.5
1.0
0.5
0.0
24
48
72
Time (h)
Untreated cells
3 + NAC
US
3 + NAC + US

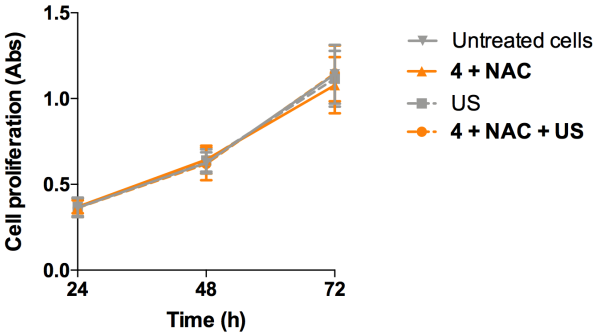
Cell proliferation (Abs)
1.5
1.0
0.5
0.0
24
48
72
Time (h)
Untreated cells
4 + NAC
US
4 + NAC + US